Multi-omic profiling reveals the ataxia protein sacsin is required for integrin trafficking and synaptic organization

Lisa E.L. Romano[1*], Wen Yih Aw[2*], Kathryn M. Hixson[2*], Tatiana V. Novoselova[1,3], Tammy M. Havener[2], Stefanie Howell[2], Bonnie Taylor-Blake[4], Charlotte L Hall[1], Lei Xing[4], Josh Beri[5,6], Suran Nethisinghe[1], Laura Perna[1], Abubakar Hatimy[7], Ginevra Chioccioli Altadonna[1], Lee M. Graves[7,8], Laura E. Herring[5,6], Anthony J. Hickey[2], Konstantinos Thalassinos[7,9], J. Paul Chapple[1†], Justin M. Wolter[2,4†]

[1] William Harvey Research Institute, Faculty of Medicine and Dentistry, Queen Mary University of London, London, EC1M 6BQ, United Kingdom.

[2] UNC Catalyst for Rare Diseases, Eshelman School of Pharmacy, The University of North Carolina at Chapel Hill, Chapel Hill, North Carolina, 27599, U.S.A.

[3] Department of Natural Sciences, Faculty of Science and Technology, Middlesex University London, NW4 4BT United Kingdom

[4] UNC Neuroscience Center, The University of North Carolina at Chapel Hill, Chapel Hill, North Carolina, 27599, U.S.A.

[5] Department of Pharmacology, University of North Carolina at Chapel Hill, Chapel Hill, NC 27599, USA

[6] UNC Michael Hooker Proteomics Center, University of North Carolina at Chapel Hill, Chapel Hill, NC 27599, USA

[7] Institute of Structural and Molecular Biology, Division of Biosciences, University College London, London, WC1E 6BT, United Kingdom.

[8] Lineberger Comprehensive Cancer Center, University of North Carolina at Chapel Hill, Chapel Hill, NC 27599, USA

[9] Institute of Structural and Molecular Biology, Birkbeck College, University of London, London, WC1E 7HX, United Kingdom

* *These authors contributed equally to this work*

† *Co-corresponding authors*

Correspondence:

Professor Paul Chapple
Centre for Endocrinology
William Harvey Research Institute
Barts and the London School of Medicine
Queen Mary University of London

Dr. Justin Wolter
UNC Neuroscience Center
University of North Carolina
Chapel Hill, North Carolina
27599

Charterhouse Square
London EC1M 6BQ
United Kingdom
Tel: +44 20 7882 6242
Email: j.p.chapple@qmul.ac.uk

U.S.A.
Tel:
Email: justin_wolter@med.unc.edu

Summary

Autosomal recessive spastic ataxia of Charlevoix-Saguenay (ARSACS) is a childhood-onset cerebellar ataxia caused by mutations in *SACS*, which encodes the protein sacsin. Cellular ARSACS phenotypes include mitochondrial dysfunction, intermediate filament disorganization, and the progressive death of cerebellar Purkinje neurons. It is unclear how the loss of sacsin function causes these deficits, or why they manifest as cerebellar ataxia. Here, we performed multi-omic profiling in sacsin knockout (KO) cells, and identified alterations in microtubule dynamics, protein trafficking, and mislocalization of synaptic and focal adhesion proteins, including multiple integrins. Focal adhesion structure, signaling, and function were affected in KO cells, which could be rescued by reducing levels of PTEN, an overabundant negative regulator of focal adhesion signaling. Purkinje neurons in ARSACS mice possessed mislocalization of ITGA1, and disorganization of synaptic structures in the deep cerebellar nucleus (DCN). Interactome analysis revealed that sacsin regulates protein-protein interactions between structural and synaptic adhesion proteins. Our findings suggest that disrupted trafficking of synaptic adhesion proteins is a causal molecular deficit underlying ARSACS.

Keywords:

ARSACS, sacsin, ataxia, proteomics, microtubules, focal adhesions, synaptic adhesion proteins, PTEN, integrin, ITGA1, Purkinje neurons

Introduction

Autosomal Recessive Spastic Ataxia of Charlevoix-Saguenay (ARSACS) is a childhood-onset neurological disease characterized by pyramidal spasticity, cerebellar ataxia, and Purkinje cell loss, that is thought to have both neurodegenerative and neurodevelopmental components (Vermeer et al., 1993). ARSACS was initially believed to be restricted to the Charlevoix-Saguenay region of Quebec, Canada, due to a founder effect mutation (Bouchard et al., 1978). But since the discovery of the causal gene, over 170 distinct mutations in *SACS* have been identified worldwide, and ARSACS is now estimated to be the second most common form of autosomal recessive cerebellar ataxia (Engert et al., 2000; Synofzik et al., 2013).

Sacsin/DNAJC29 is ubiquitously expressed, but has especially high expression in large neurons in brain regions associated with motor systems, including layer-V pyramidal neurons in the motor cortex, and cerebellar Purkinje cells (Saunders et al., 2018). Sacsin is a large 520 kDa modular protein with multiple domains that implicate it in molecular chaperone and protein quality control systems (Anderson et al., 2010; Parfitt et al., 2009). These include an N-terminal ubiquitin-like domain, regions of homology to the ATPase domain of Hsp90, and a functional J-protein domain, suggesting that sacsin has the ability to modulate Hsp70 chaperone activity. However, the large size of sacsin has hampered biochemical and structural investigations into its function. Patient derived fibroblasts and sacsin KO cell models demonstrate reorganization of the vimentin intermediate filament cytoskeleton, altered mitochondrial network dynamics and trafficking, decreased mitochondrial respiration, and increased mitochondrial stress (Bradshaw et al., 2016; Duncan et al., 2017a; Gentil et al., 2019; Girard et al., 2012; Lariviere et al., 2015). Aptamer-based proteomics in sacsin KO SH-SY5Y neuroblastoma cells also found altered expression of proteins involved in synaptogenesis and cell engulfment (Morani et al., 2020). *Sacs*$^{-/-}$ mice recapitulate the motor deficits and cerebellar atrophy observed in ARSACS patients, and undergo progressive age-dependent loss of cerebellar Purkinje neurons. These neurons demonstrate abnormal bundling of non-phosphorylated neurofilament in somatodendritic regions (Lariviere *et al.*, 2015; Lariviere et al., 2019), and changes to the structure of Purkinje neuron synapses in the DCN (Ady et al., 2018).

While these cellular phenotypes may affect neuronal function and survival, their precise relationship to neurodegeneration in ARSACS is unclear. More broadly, altered mitochondrial dynamics and intermediate filament phenotypes are frequent in diverse neurodegenerative diseases (Didonna and Opal, 2019; Stanga et al., 2020). Whether these phenotypes are causal, or merely components of a conserved neurodegenerative cascade, is an important unanswered

question in many neurodegenerative diseases (Gan et al., 2018). Here, we take a multi-omic approach to determine how the loss of sacsin causes these phenotypes, and why this disease manifests as a cerebellar ataxia. Our data suggests that altered trafficking of synaptic adhesion proteins is a causal molecular deficit in ARSACS.

Results

Comprehensive proteomics of sacsin KO cells

To understand the molecular deficiencies in ARSACS, we generated a sacsin KO human SH-SY5Y cell line (Fig. S1a), which is widely used to model neurodegenerative diseases (Xicoy et al., 2017). Consistent with ARSACS patient fibroblasts (Duncan *et al.*, 2017a) and *Sacs*$^{(-/-)}$ mice (Lariviere *et al.*, 2015), KO cells had abnormal bundling and asymmetric partitioning of multiple IFs, including vimentin (Fig. 1a), neurofilament heavy, and peripherin (Fig. S1b-e). As phosphorylation is a key post-translational modification controlling intermediate filament assembly and disassembly (Snider and Omary, 2014), we performed quantitative proteomic and phosphoproteomic profiling of sacsin KO cells (Supplementary Table 1). We identified decreased abundance of several proteins previously described in ARSACS patient fibroblasts, including vimentin, the mitochondrial protein ATP5J, and the autophagy regulated scaffold SQSMT1/p62 (Duncan *et al.*, 2017a) (Fig. 1b, Supplementary Table 1). Among the overabundant proteins were the tau-tubulin kinase 1 (TTBK1) and microtubule associated protein tau (MAPT) (Fig. 1c-f), which was hyperphosphorylated at several sites (Fig. S1f, Fig. 1g,h, Supplementary Table 1). To assess the functional significance of each phosphosite, we analyzed our data in light of a recent machine learning approach which estimated the effects of individual phosphosites on organism fitness (Ochoa et al., 2020). This analysis identified several highly functional hypophosphorylated residues in vimentin and the nuclear lamina intermediate filaments LMNA/LMNB2, which is intriguing considering that ARSACS neurons have altered nuclear shape and positioning (Duncan *et al.*, 2017a) (Supplementary Table 1, Fig. 1i). Other hypophosphorylated proteins included the focal adhesion protein zyxin (ZYX), and ataxin 2-like protein (ATXN2L). In addition to tau, several other microtubule regulating proteins were hyperphosphorylated, including the primary cilia protein ARL3 (Zhou et al., 2006), and the scaffold stathmin (STMN1), which promotes microtubule assembly in a pS16 dependent fashion (Di Paolo et al., 1997) (Fig. 1i). We next analyzed changes in phosphorylation corrected for changes in total protein levels (Fig. S1g, Supplementary Table 1). The most hypophosphorylated proteins were RPS6, NLM1, and ATXN2L, which have been implicated in neuronal autophagy, and likely reflect increased autophagy in sacsin KO cells (Duncan et al., 2017b; Klionsky et al., 2021; Tang et al., 2021) (Duncan *et al.*, 2017b; Key et al., 2020). The most hyperphosphorylated residues were again in microtubule related proteins, such as HN1/JPT1 and ARL3 (Fig. S1g). In all, these results suggest that altered phosphorylation may be a contributing factor to cellular ARSACS phenotypes.

Kinases are attractive drug targets (Krahn et al., 2020), but are typically lowly expressed and difficult to detect with standard proteomics. Therefore, we enriched for kinases using multiplexed kinase inhibitor beads, and performed quantitative mass-spectrometry (Cooper et al., 2013). The kinome was broadly altered in sacsin KO cells (Fig. S1h,i, Supplementary Table 1), with affected kinases spread among all kinase families (Fig. 1j). Interestingly, specific families were generally misexpressed in similar directions. For example, the tyrosine kinase family (TK) members were generally downregulated, while CMGC family members were generally upregulated (Fig. 1j). Strikingly, we identified 10 overexpressed kinases which directly phosphorylate tau at specific residues which were hyperphosphorylated in sacsin KO cells (Fig. 1k, Fig. S1h). The most overabundant kinase, BRSK2, and additional CAMK family members MARK1/2/3, all phosphorylate Ser262 in the microtubule binding domain of tau (Ando et al., 2016; Kishi et al., 2005) (Fig. 1k-n). Phosphorylation of tau Thr231 by DYRK1A is also associated with the detachment of tau from microtubules (Coutadeur et al., 2015; Sengupta et al., 1998). In pathological settings, tau overabundance and hyperphosphorylation can cause the aggregation of insoluble tau and the formation of neurofibrillary tangles. However, biochemical quantification of tau aggregation did not find evidence of increased accumulation in either undifferentiated, or neuronally differentiated sacsin KO cells (Fig. S1j). However, independent of aggregation, dysregulated tau phosphorylation alters microtubule stability, interferes with motor protein function, and disrupts axonal trafficking (Dixit et al., 2008; Ikezu et al., 2020; Stoothoff and Johnson, 2005). Combined with the altered phosphorylation of other microtubule related proteins (Fig. 1i), this data suggests that microtubule structure or function may be altered in sacsin KO cells.

Microtubule organization and dynamics are altered in sacsin KO cells

We next sought to determine whether microtubule structure and function is affected in sacsin KO cells. We found that cage-like vimentin bundles form around gamma-tubulin, a marker of the microtubule organizing center (MTOC), which is a central hub for microtubule nucleation and cargo transport (Martin and Akhmanova, 2018) (Fig. 2a, Fig. S2a). Acetylated alpha-tubulin, a microtubule stabilizing post-translational modification, was increased in sacsin KO cells, without affecting total alpha-tubulin distribution or levels (Fig. S2b, Fig. 2b,c). To assess microtubule dynamics we treated cells with the microtubule destabilizer nocodazole, and found enhanced microtubule polymerization following nocodazole washout (Fig. 2d,e). Sacsin KO cells also demonstrated increased microtubule polymerization and disordered movements

as assessed by live cell imaging of the microtubule plus-end binding protein EB1:GFP (Fig. 2f, Fig. S2e, Supplementary Video 1,2).

Mitochondrial trafficking in neurons is dependent on microtubules (Melkov and Abdu, 2018), and Tau overexpression and hyperphosphorylation can cause decreased mitochondrial trafficking (Ando *et al.*, 2016; Lopes et al., 2017; Reddy, 2011), build-up of mitochondria around the MTOC (Ebneth et al., 1998), and DRP1 mislocalization and reduced mitochondrial fission (DuBoff et al., 2012; Manczak and Reddy, 2012). In ARSACS, mitochondria also accumulate around proximal dendrites (Girard *et al.*, 2012) and exhibit reduced DRP1 dependent fission (Bradshaw *et al.*, 2016). We observed occlusion of mitochondria around vimentin bundles (Fig. S2c), with no alterations in the actin cytoskeleton (Duncan *et al.*, 2017a) (Fig. S2d). To assess how these alterations affect mitochondria in neurons, we performed neuronal differentiation of SH-SY5Y cells (Shipley et al., 2016). While WT and sacsin KO cells expressed indistinguishable levels of neuronal markers, neurites were fewer and shorter in sacsin KO cells (Fig. S2f-i), contained fewer mitochondria (Fig. S2j), and had diminished mitochondrial movement (Fig. S2k, Supplementary Video 3). Our proteomics data also identified several hyperphosphorylated kinesin proteins, which shuttle mitochondria along microtubule tracts (Frederick and Shaw, 2007) (Supplementary Table 1). In all, these results demonstrate that the loss of sacsin affects microtubule structure, dynamics, and function.

Focal adhesion organization and dynamics are disrupted in sacsin KO cells

To more systematically characterize our proteomic datasets, we performed gene ontology (GO) analysis for the total proteome and phosphoproteome (Fig. 3a,b, Supplementary Table 2). The top associated terms in the proteome were related to ‘focal adhesions’, including ‘integrin signaling’, ‘cell-matrix adhesions’, and ‘cadherin binding’. ‘Focal adhesions’ was also a top term in phosphoproteome, suggesting that focal adhesion proteins are affected both at the total protein and post-translational levels. Focal adhesions are plasma membrane-associated macromolecular assemblies that physically link the intracellular cytoskeleton and extracellular matrix (ECM). Focal adhesions are composed of integrin receptors bridging the ECM with actin bundles, which interact with microtubules and IFs to coordinate dynamic regulation of focal adhesion structure (Ezratty et al., 2005; Leube et al., 2015; Seetharaman and Etienne-Manneville, 2019). In the brain, focal adhesions are critical for structural remodeling during axon growth, synapse formation, and maintenance (Kilinc, 2018). Immunolabelling for the core focal

adhesion proteins paxillin and vinculin revealed decreased focal adhesion number, area, and aspect ratio in sacsin KO cells (Fig. 3c, Fig. S3a-g, Supplementary Table 1). Total levels of these proteins were unaffected in sacsin KO cells (Fig. S3h, Supplementary Table 1). While paxillin is primarily localized at focal adhesions, it also is known to interact with the MTOC (Robertson and Ostergaard, 2011), and we observed perinuclear accumulation of paxillin coinciding with the vimentin bundle (Fig. S3a). Microtubules regulate vinculin localization to focal adhesions (Ng et al., 2014), and we found reduced vinculin and vimentin dynamics in sacsin KO cells using fluorescence recovery after photobleaching (FRAP) (Fig. 3d-f). We next removed cell bodies with hypotonic shock, leaving only the structural remnants of cell/ECM interactions, and again found reduced vinculin structures, suggesting that the mislocalization of adhesion proteins also results in decreased cell/ECM interactions (Fig. S3i-l). These findings were consistent in sacsin KO HEK293 cells, which were generated using an alternate CRISPR/Cas9 genome editing strategy (Duncan *et al.*, 2017a) (Fig. S3m-q). Our proteomics data also revealed decreased levels of several integrin proteins (Fig. 3g). Localization of ITGAV to focal adhesions was diminished in sacsin KO cells (Fig. 3h), while ITGA6 was sequestered in the vimentin bundle (Fig. 3i). In all, this data suggests that the trafficking, structure, and function of multiple focal adhesion proteins is affected in sacsin KO cells.

Modulating PTEN-FAK signaling rescues cellular deficits in sacsin KO cells

Beyond providing structural support for cells, focal adhesions are enriched with many signaling proteins, which transmit signals from the extracellular milieu to effectors in the cytoplasm and nucleus. A master regulator of focal adhesion signaling is the focal adhesion kinase (FAK/PTK2) (Sulzmaier et al., 2014). FAK is recruited to integrin adhesion complexes through interactions with paxillin (Brown et al., 1996), and is activated via autophosphorylation at Tyr397 following integrin receptor binding to the ECM (Zhao and Guan, 2011). FAK regulates neuronal outgrowth and synapse formation by phosphorylating multiple downstream effectors of focal adhesion signaling (Rico et al., 2004) (Fig. 4a). Although total levels of FAK were unaltered in sacsin KO cells, phosphorylated FAK (pFAK) was significantly reduced, as was its localization to focal adhesions (Fig. 4b,c, Fig. S4a,b). JNK and paxillin, downstream targets of activated pFAK (Zhao and Guan, 2011), were also hypophosphorylated, without corresponding changes in protein levels (Fig. 4b, Fig. S4c-g, Supplementary Table 1). This data suggests that FAK signaling is suppressed in sacsin KO cells, possibly through disengagement with focal adhesions.

We next considered the mechanism by which FAK signaling is suppressed in sacsin KO cells. The phosphatase PTEN, which dephosphorylates FAK and negatively regulates FAK activity (Tamura et al., 1999), was elevated in sacsin KO cells (Fig. 4b, Fig. S4h). To investigate whether increased PTEN is a general consequence of intermediate filament disorganization, we treated WT SH-SY5Y cells with simvastin (Trogden et al., 2018), which induced bundling and perinuclear accumulation of vimentin, but did not affect PTEN levels (Fig. S4i-k). Conversely, reducing PTEN by siRNA-mediated knockdown to WT levels in sacsin KO cells (Fig. S4l,m), increased pFAK and pPAX (Fig. 4d, S4l,m), reduced the frequency of perinuclear vimentin accumulation (Fig. 4e,f), and increased the number of focal adhesions (Fig. 4e,g). Focal adhesions play an important role in the migratory behaviors of cells (De Pascalis and Etienne-Manneville, 2017). Sacsin KO cells exhibited migration deficits in scratch and transwell migration assays (Fig. S4 n-q), which were rescued by PTEN knockdown (Fig. S4r,s). Together these results indicate that increased PTEN activity contributes, at least in part, to the intermediate filament and focal adhesion phenotypes in sacsin KO cells. Furthermore, our data suggests that modulating this pathway may ameliorate molecular deficits associated with ARSACS.

Membrane bound synaptic adhesion molecules are mislocalized in sacsin KO cells

Focal adhesions act as signal transduction hubs to integrate information from the outside of the cell to the inside. Some focal adhesion proteins, including paxillin and zyxin (Fig. 1i), can shuttle to the nucleus and function as transcriptional coregulators in a phosphorylation dependent manner (Dong et al., 2009; Suresh Babu et al., 2012). Interestingly, GO term analysis for proteins with altered phosphorylation were highly enriched for terms related to RNA processing, including ‘RNA binding’, ‘cytoplasmic stress granules’, ‘spliceosome’, and ‘nuclear body’ (Fig. 3b, Supplementary Table 2), suggesting that the altered phosphorylation landscape may be affecting the transcriptome. Therefore, we next performed RNA-seq of neuronally differentiated SH-SY5Y cells (Fig. S5a, Supplementary Table 3). We found 876 differentially expressed genes (FDR<0.05, $\log_2$ f.c. -/+ 0.4), suggesting the loss of sacsin has profound effects on the transcriptome (Fig. S5a). Protein interaction mapping (Szklarczyk et al., 2019) revealed altered expression of multiple ECM proteins, integrins, and regulators of integrin activation (Fig. S5b). Interestingly, changing the total levels or activity of specific integrins can affect the expression of other integrin subunits, a phenomenon called ‘integrin crosstalk’ (Samarzija et al., 2020). The observation that multiple integrins were affected at both the protein

and RNA levels suggests that altered integrin localization may activate regulatory feedback loops that affect the expression of genes that play a role in membrane based signaling. Indeed, GO term analysis of differentially expressed genes identified terms implicating membrane related processes, including ‘post-synaptic membrane’, ‘axon terminus’, ‘endomembrane system’, and ‘cytoplasmic vesicle membrane’ (Fig. S5c). In all, this data suggests that the altered phosphorylation landscape in sacsin KO cells affects mRNAs encoding for proteins involved in membrane related processes.

Cell surface proteins are frequently underrepresented in proteomics experiments due to low expression and biochemical properties (Bausch-Fluck et al., 2015). Indeed, while 26% of the genes detected by RNA-seq were detected in the proteome, only 11% of differentially expressed genes (which were enriched for membrane proteins) were detected in the proteome (Fig. S5d). Therefore, to better characterize membrane and surface proteins, we incubated live cells with biotin, labelling cellular and exosomal membrane/surface proteins, followed by neutravidin purification and analysis by quantitative mass-spectrometry (Nunomura et al., 2005) (Fig. 5a, Supplementary Table 1). This approach identified an additional 870 proteins not in our initial proteomic datasets (Fig. S5e, Fig. 5b). Proteins with altered surface expression in sacsin KO cells included several signaling receptors (FGFR1, LRP4, NRP2), and GTP binding proteins involved in signal transduction (GNG2, GNG8). The most overabundant membrane protein was neurofascin (NFASC), a neuronal adhesion protein that has been linked to movement disorders and cerebellar ataxia (Kvarnung et al., 2019; Smigiel et al., 2018) (Fig. 5c). We next compared membrane proteins found in both proteomic and surfaceome datasets, reasoning that conflicting levels between cell surface and total protein levels could reflect improper membrane recycling, precocious membrane localization, or deficits in membrane-bound trafficking. Many proteins with altered surface levels showed no, or even opposing change in total protein levels (Fig. 5d, Supplementary Table 1). Among the most mislocalized proteins were synaptic adhesion proteins, including multiple integrins (ITGA1, ITGB1, ITGA3), neuronal cell adhesion molecules (NRCAM, CNTN1, LSAMP), the focal adhesion regulator RET/GFRA3 heterodimer, the microtubule binding protein DCX, and AHNAK, a 700 kDa scaffolding protein with diverse yet poorly understood function (Davis et al., 2015) (Fig. 5d).

GO term analysis of proteins with altered surface levels suggested deficits in processes related to vesicle packaging and transport (Fig. 5e). These included eight exosomal Rab proteins, which were increased in the surfaceome and not affected at the total protein level (Fig. S5f, Supplementary Table 1). Rabs are a diverse family of GTPases that coordinate multiple

aspects of membrane protein trafficking, including focal adhesion turnover, and integrin endo/exocytosis (Moreno-Layseca et al., 2019). Specific Rabs also regulate trafficking between the Golgi and the endosomal network (RAB8A, RAB10), bidirectional Golgi/ endoplasmic reticulum (ER) trafficking (RAB2A, RAB18), and EGFR internalization (RAB7A) (Bakker et al., 2017; Galea and Simpson, 2015). Kinome profiling also identified multiple regulators of Rab activity and trafficking, including PIK3R4 and PIK3C3, which regulate PTEN activity through localization to vesicles in a microtubule dependent fashion (Naguib et al., 2015) (Fig. 1j, Supplementary Table 1).

To assess trafficking and localization deficits in sacsin KO cells we investigated the localization of the ECM protein fibronectin, which is processed and packaged into vesicles in the ER and Golgi (Kii et al., 2016), and trafficked to the cell periphery along microtubules (Noordstra and Akhmanova, 2017). Fibronectin was not affected in any of our proteomics datasets, allowing us to investigate mislocalization independent of changes in protein level or phosphorylation. In WT HEK293 cells fibronectin puncta were organized in ‘chains’, which appear collapsed around the vimentin bundle in sacsin KO cells (Fig. 5f). Staining for the ER marker KDEL revealed that fibronectin is retained in the ER in HEK293 and SH-SY5Y sacsin KO cells (Fig. 5g, Fig. S5g), suggesting that membrane bound trafficking is affected in sacsin KO cells.

We next used Ingenuity Pathway Analysis (IPA) to assess whether the misregulated cell surface proteins are associated with any pathological conditions. Resoundingly, the terms were associated with disease traits reminiscent of ARSACS, including movement disorders, neurodegeneration, and progressive neurological disorder (Fig. 5h). Notably, three of the most mislocalized proteins, NFASC, NRCAM, and CNTN1, form molecular complexes that are important for axon guidance (Pollerberg et al., 2013), maintenance of synapses by astrocytes (Takano et al., 2020), and interactions between Purkinje neuron axons and glia (Bhat et al., 2001). KO mice or humans which harbor mutations in each of these genes develop cerebellar ataxias with features that resemble ARSACS (see Discussion).

Integrin trafficking and synaptic structure are affected in ARSACS mice

Cerebellar atrophy is an early clinical feature of ARSACS (Martin et al., 2007; Synofzik *et al.*, 2013). In the ARSACS mouse model, the progressive death of Purkinje neurons begins around P90 (Lariviere *et al.*, 2015), and is well underway by P120 (Fig. 6a). To determine

whether any of the proteins which were mislocalized in our sacsin KO cell model were also affected in the brain, we focused on mice at P60, which is when behavioural deficits first emerge, but prior to Purkinje neuron death (Lariviere *et al.*, 2015). ITGA1, which was among the most mislocalized proteins in sacsin KO cells (Fig. 5d), is normally localized in nuclear Cajal bodies, and Purkinje axons in *Sacs*$^{(+/-)}$ mice (Fig. 6b-c). However, in *Sacs*$^{(-/-)}$ mice, we observed striking accumulation of ITGA1 in the soma and dendritic trunk (Fig. 6b-d). Axonal swelling near to the Purkinje neuron soma is a consistent feature in *Sacs*$^{(-/-)}$ mice (Lariviere *et al.*, 2015), and we also observe ITGA1 accumulation in these structures (Fig. S6a). In contrast, we observed a decrease of ITGA1 in Purkinje neuron axon tracts (Fig. 6e-g), suggesting that ITGA1 trafficking along axon tracts is diminished.

Purkinje axons synapse onto neurons in the deep cerebellar nucleus (DCN), which in turn project to multiple brain regions. As the primary output hub of the cerebellum (Ito, 2002), alterations in the Purkinje-DCN circuit have substantial effects on both motor and non-motor processes (Baek et al., 2022; Sathyamurthy et al., 2020), and are observed in multiple neurodegenerative ataxias (Barron et al., 2018; Feng et al., 2022; Walter et al., 2006). We observed striking disorganization of Purkinje neurons synapses in the DCN in *Sacs*$^{(-/-)}$ mice at P60 (Fig. 6h) and P120 (Fig. S6b,c), in agreement with a previous report (Ady *et al.*, 2018). The number of Purkinje synapses on each DCN neuron was reduced in *Sacs*$^{(-/-)}$ mice (Fig. 6i), while the size of Purkinje foci apposed to DCN neurons was substantially increased (Fig. 6j). We observed accumulation of ITGA1 in large CALB+ structures in *Sacs*$^{(-/-)}$ mice, suggesting that while long range ITGA1 trafficking is not altogether abolished in *Sacs*$^{(-/-)}$ mice, ITGA1 does accumulate in these pathological swellings (Fig. S6d,e). Interestingly, we also observed increased ITGA1 staining in the cell bodies of DCN neurons (Fig. 6k, S6f), and accumulation of ITGA1 in the large diameter dendrites of DCN neurons (Fig. 6k,l). This pattern was similar to the dendritic ITGA1 accumulation seen in Purkinje neurons (Fig. 6c), suggesting that altered protein localization is not unique to Purkinje neurons. As DCN neurons project throughout the brain, the physical disruption between Purkinje and DCN neurons suggests that cerebellar output to multiple brain regions may be directly affected in ARSACS.

The loss of sacsin disrupts protein-protein interactions

To identify how the loss of sacsin causes abnormal protein trafficking, we performed quantitative label-free mass spectrometry of endogenous sacsin co-immunoprecipitated (co-IP) from WT SH-SY5Y cells. KO cells were also used to control for non-specific protein pulldown.

Our analysis identified 96 proteins as putative sacsin interactors, including vimentin and vinculin (Supplementary Table 4). Immunofluorescence revealed sacsin puncta in and around vinculin positive focal adhesions (Fig. S7a,b), and in close proximity to vimentin structures, with sacsin often being between them (Fig. 7a). Reciprocal co-IP experiments confirmed interactions between sacsin, vimentin and vinculin, but the interaction between vimentin and vinculin was dramatically reduced in sacsin KO cells (Fig. 7b). NFASC has been reported to interact with vimentin (Sistani et al., 2013), leading us to wonder whether NFASC may also interact with focal adhesion proteins. Co-IP experiments identified an interaction between NFASC and vinculin, which was dramatically reduced in sacsin KO cells (Fig. 7c). These results suggest that sacsin promotes the formation and/or stabilization of adhesion protein interactions.

To identify central proteins which may explain the cellular phenotypes in sacsin KO cells, we performed STRING network analysis (Szklarczyk et al., 2019). We considered all proteins altered in any of our proteomics datasets, and assessed only high confidence physical or regulatory interactions. K-means clustering of network interactions identified three clusters, which highlight complementary pathways by which sacsin contributes to cell structure and signaling (Fig. 7d). Central to cluster 1 is the interaction between sacsin and intermediate filament proteins, which interact with a variety of cell surface receptors. Combined with our biochemical experiments, this suggests that the loss of sacsin leads to improper localization of adhesion proteins to the plasma membrane, through decreased protein interactions between IFs, adaptors, and adhesion proteins. PTEN regulates several of these proteins, suggesting additional targets beyond FAK which may contribute to sacsin KO phenotypes. The network also highlighted the microtubule associated kinase MAST1 (Fig. 1j, increased expression), which stabilizes PTEN (Valiente et al., 2005), and is protected from proteasomal degradation by the sacsin interactor HSP90B1 (Pan et al., 2019).

Cluster 2 is composed of the interaction between sacsin, chaperone network proteins, and microtubules, which in concert regulate membrane protein processing, trafficking, and localization (McClellan et al., 2007). Multiple HSP chaperones were part of the sacsin interactome (Fig. 7d), including the marker of ER stress HSPA5/BIP, and several HSP90 proteins, which can stabilize FAK, modulate cell migration (Xiong et al., 2014), and regulate microtubules (Quinta et al., 2011). Recent evidence suggests HSP90 is essential for microtubule acetylation (Wu et al., 2020), suggesting that the loss of sacsin may alter microtubule stability via HSP proteins (Fig. 2d,e). HSP proteins also regulate Rab proteins (Chen and Balch, 2006) (cluster 3), which have diverse roles in vesicular trafficking, including

PTEN and EGFR trafficking (Shinde and Maddika, 2016). Rabs are highly enriched in synapses, play key roles in endo- and exocytosis, and are linked to many neurodegenerative diseases (Kiral et al., 2018). The increased surface abundance of multiple Rab proteins without corresponding changes in total Rab levels (Fig. 7d) is consistent with the precocious microtubule stability and dynamics we observe in sacsin KO cells (Fig. 2). GO term analysis revealed that 65% of sacsin interacting proteins are involved in exosome related processes, with additional interactors being implicated in unfolded protein binding (HSPs) and focal adhesions (Fig. S7c). In all, these results suggest that sacsin plays a critical role in functionally bridging protein quality control systems, microtubule dependent vesicular transport, and membrane localization of adhesion proteins.

Discussion

This study identifies sacsin as a central regulator of multiple aspects of cellular structure, including intermediate filament architecture, microtubules, protein trafficking, and focal adhesions. The complex and intertwined relationships between these processes complicates our understanding of their precise pathophysiological relevance, but our study raises some intriguing possibilities. Sacsin possesses a functional J domain, which interacts with HSP70 chaperone proteins (Genest et al., 2019; Parfitt *et al.*, 2009) (Fig. 7d). HSP proteins play a role in ubiquitin dependent turnover of IFs (Gavriilidis et al., 2018), and neurofilament bundling in ARSACS neurons can be rescued by HSP expression (Gentil *et al.*, 2019). Sacsin also possesses an ATPase domain with homology to HSP90 proteins. The sacsin interactor HSP90B1 stabilizes FAK (Xiong *et al.*, 2014), suggesting that restoring FAK signaling may rescue intermediate filament structure through HSP activity (Fig. 4,7d). It is also possible that sacsin transiently interacts with HSP90 regulated kinases, such as FAK (Xiong *et al.*, 2014), and has a more direct role at focal adhesions. HSP70/90 complexes bind to microtubules in an acetylation dependent fashion (Giustiniani et al., 2009), and interact with hyperphosphorylated tau to increase tau's interaction with microtubules (Lackie et al., 2017). Since HSPs are known to regulate all of the protein clusters with deficits in sacsin KO cells (Fig. 7d), we hypothesize that the interaction between HSPs and sacsin may be an especially critical interaction that is lost in ARSACS. Furthermore, as illustrated by sacsin's mediation of the interaction between IFs and focal adhesions, changes in additional as yet uncharacterized protein-protein interactions may explain specific ARSACS phenotypes, such as disrupted autophagy, nuclear morphology, and aberrant localization of mitochondria.

Integrins play key roles in modulating axon outgrowth, dendritic arborization, and regulating synaptic structure and function (Park and Goda, 2016). More specifically, multiple integrins and pFAK are localized to dendritic spines in cultured Purkinje neurons, where they regulate spine remodeling (Heintz et al., 2016). However, little is known about the role of ITGA1 in the brain (Murase and Hayashi, 1998), and the lack of a mechanistic connection between ITGA1 localization and the changes to synaptic structure in ARSACS mice is a limitation of our findings. As multiple levels of data suggest that integrins as a class are affected in sacsin KO cells (proteomics, transcriptomics, and surfaceomics), exploring the localization of additional integrin subunits may shed light on this question. Furthermore, integrins are in general most highly expressed during brain development (Nieuwenhuis et al., 2018). Thus, defining when changes in integrin mislocalization and synaptic structure first emerge may yield important insight into the pathomechanistic origins of ARSACS.

Why do mutations in sacsin, which is expressed throughout the brain, present as a cerebellar ataxia? Proteins whose abundance or localization are altered in sacsin KO cells, and which also cause cerebellar ataxia, could suggest a causal molecular deficiency in ARSACS. The interactions between NFASC, NRCAM, and CNTN1 are critical for brain development, and mutation of each causes phenotypes reminiscent of ARSACS. *Cntn1* KO mice have deficits in axon guidance and develop cerebellar ataxia (Berglund et al., 1999). *Nrcam* KO mice have phenotypes only in lobules 4/5 of the cerebellar vermis (Sakurai et al., 2001), which are also specifically affected in ARSACS (Ady *et al.*, 2018; Lariviere *et al.*, 2015; Lariviere *et al.*, 2019). Lastly, human mutations in *NFASC* which selectively remove the 155kD glial isoform cause congenital hypotonia, demyelinating neuropathy (as in ARSACS) and severe motor coordination defects (Smigiel *et al.*, 2018), while mutations of the neuron specific 186kD NFASC isoform cause cerebellar ataxia (Kvarnung *et al.*, 2019). These convergent phenotypes lead us to hypothesize that improper localization of synaptic cell adhesion molecules may be a causal molecular deficiency in ARSACS.

In development, if an axon fails to make productive synaptic connections and receive neurotrophic input from nearby cells, molecular cascades are activated which cause localized pruning of non-productive axonal branches (Dekkers et al., 2013). This process, which initiates at the synapse and advances to the cell body, is referred to as the dying back model, and can cause neuronal death (Raff et al., 2002). Although this is a normal mechanism to ensure proper wiring of the nervous system in the face of stochastic errors in axon guidance, this process is co-opted in many neurodegenerative disorders, including ALS (Dadon-Nachum et al., 2011),

Alzheimer's disease (Salvadores et al., 2017), Huntington's disease (Han et al., 2010), Parkinson's disease (Dauer and Przedborski, 2003), and hereditary spastic paraplegias (Fink, 2013). A common molecular thread across these diseases is microtubule based axonal transport (Morfini et al., 2009). Indeed, many of the proteins implicated in the above diseases were also identified in this study (tau, tau kinases, Rabs, synaptic adhesion proteins, etc.). This leads us to speculate that the loss of sacsin alters microtubule function, resulting in improper trafficking of synaptic adhesion proteins, deficits in synaptic structure, activation of axonal degeneration, and ultimately Purkinje neuron death. A mechanistic exploration of this hypothesis will be necessary for the development of rationally designed therapeutic strategies aimed at delaying or preventing ARSACS progression.

ACKNOWLEDGEMENTS

We express our gratitude to Sonia Gobeil and the ARSACS patient community. This work was supported by grants to J.P.C and J.M.W. from the Fondation de l'Ataxie Charlevoix-Saguenay. We thank Thomas Sterns, Karim Gilbert, Natalie Barker, and Dennis Goldfarb for technical assistance. We thank Dr. Stefan Strack for generously providing ARSACS mice. We also thank Dr. Mark Zylka and Dr. Jason Stein for their advice and support. JPC was supported by the BBSRC (BB/R003335/1) and Ataxia UK. JMW was supported by grants from the National Institute for Child Health and Human Development (NICHD; T32HD040127) and a Pfizer-NCBiotech Postdoctoral Fellowship in Gene Therapy. LMG is supported by NIH R01 GM138520. The UNC Catalyst for Rare Diseases gratefully acknowledges the support of the Eshelman Institute for Innovation. This research is based in part upon work conducted using the UNC Proteomics Core Facility, which is supported in part by P30 CA016086 Cancer Center Core Support Grant to the UNC Lineberger Comprehensive Cancer Center. Confocal microscopy was performed using a microscope funded by Barts Charity (MGU0293), and at the UNC Neuroscience Microscopy Core (RRID:SCR_019060), supported, in part, by funding from the NIH-NINDS Neuroscience Center Support Grant P30 NS045892 and the NIH-NICHD Intellectual and Developmental Disabilities Research Center Support Grant U54 HD079124.

AUTHOR CONTRIBUTIONS

JMW and JPC conceived of the study. JMW, JPC, and LELR analyzed data and prepared the manuscript. SN, TMH, and JMW created sacsin KO neuroblastoma lines. LMG aided in experimental design and provided reagents for proteomics experiments. AJH and KT provided reagents and experimental oversight. WYA, KMH, BTB, LX, and JMW performed histology. SH, TMH, and WA managed the mouse colony. KMH, TMH, SH, JB, LEH, and JMW performed quantitative proteomics experiments. TVN and CLH performed RNAseq, KMH and JMW analyzed the data. TVN and CLH performed the sacsin interactome experiments. AH and KT performed co-IP MS experiments. LELR, WYA, KMH, TVN, TMH, SH, LP, JMW, and GCA performed cell biology experiments.

REFERENCES

Ady, V., Toscano-Marquez, B., Nath, M., Chang, P.K., Hui, J., Cook, A., Charron, F., Lariviere, R., Brais, B., McKinney, R.A., and Watt, A.J. (2018). Altered synaptic and firing properties of cerebellar Purkinje cells in a mouse model of ARSACS. The Journal of physiology *596*, 4253-4267. 10.1113/JP275902.

Anderson, J.F., Siller, E., and Barral, J.M. (2010). The sacsin repeating region (SRR): a novel Hsp90-related supra-domain associated with neurodegeneration. Journal of molecular biology *400*, 665-674. 10.1016/j.jmb.2010.05.023.

Ando, K., Maruko-Otake, A., Ohtake, Y., Hayashishita, M., Sekiya, M., and Iijima, K.M. (2016). Stabilization of Microtubule-Unbound Tau via Tau Phosphorylation at Ser262/356 by Par-1/MARK Contributes to Augmentation of AD-Related Phosphorylation and Abeta42-Induced Tau Toxicity. PLoS genetics *12*, e1005917. 10.1371/journal.pgen.1005917.

Baek, S.J., Park, J.S., Kim, J., Yamamoto, Y., and Tanaka-Yamamoto, K. (2022). VTA-projecting cerebellar neurons mediate stress-dependent depression-like behaviors. eLife *11*. 10.7554/eLife.72981.

Bakker, J., Spits, M., Neefjes, J., and Berlin, I. (2017). The EGFR odyssey - from activation to destruction in space and time. Journal of cell science *130*, 4087-4096. 10.1242/jcs.209197.

Barron, T., Saifetiarova, J., Bhat, M.A., and Kim, J.H. (2018). Myelination of Purkinje axons is critical for resilient synaptic transmission in the deep cerebellar nucleus. Scientific reports *8*, 1022. 10.1038/s41598-018-19314-0.

Bausch-Fluck, D., Hofmann, A., Bock, T., Frei, A.P., Cerciello, F., Jacobs, A., Moest, H., Omasits, U., Gundry, R.L., Yoon, C., et al. (2015). A mass spectrometric-derived cell surface protein atlas. PLoS One *10*, e0121314. 10.1371/journal.pone.0121314.

Berglund, E.O., Murai, K.K., Fredette, B., Sekerkova, G., Marturano, B., Weber, L., Mugnaini, E., and Ranscht, B. (1999). Ataxia and abnormal cerebellar microorganization in mice with ablated contactin gene expression. Neuron *24*, 739-750. 10.1016/s0896-6273(00)81126-5.

Bhat, M.A., Rios, J.C., Lu, Y., Garcia-Fresco, G.P., Ching, W., St Martin, M., Li, J., Einheber, S., Chesler, M., Rosenbluth, J., et al. (2001). Axon-glia interactions and the domain organization of myelinated axons requires neurexin IV/Caspr/Paranodin. Neuron *30*, 369-383. 10.1016/s0896-6273(01)00294-x.

Bouchard, J.P., Barbeau, A., Bouchard, R., and Bouchard, R.W. (1978). Autosomal recessive spastic ataxia of Charlevoix-Saguenay. Can J Neurol Sci *5*, 61-69.

Bradshaw, T.Y., Romano, L.E., Duncan, E.J., Nethisinghe, S., Abeti, R., Michael, G.J., Giunti, P., Vermeer, S., and Chapple, J.P. (2016). A reduction in Drp1-mediated fission compromises mitochondrial health in autosomal recessive spastic ataxia of Charlevoix Saguenay. Human molecular genetics *25*, 3232-3244. 10.1093/hmg/ddw173.

Brown, M.C., Perrotta, J.A., and Turner, C.E. (1996). Identification of LIM3 as the principal determinant of paxillin focal adhesion localization and characterization of a novel motif on paxillin directing vinculin and focal adhesion kinase binding. The Journal of cell biology *135*, 1109-1123. 10.1083/jcb.135.4.1109.

Chen, C.Y., and Balch, W.E. (2006). The Hsp90 chaperone complex regulates GDI-dependent Rab recycling. Molecular biology of the cell *17*, 3494-3507. 10.1091/mbc.e05-12-1096.

Cooper, M.J., Cox, N.J., Zimmerman, E.I., Dewar, B.J., Duncan, J.S., Whittle, M.C., Nguyen, T.A., Jones, L.S., Ghose Roy, S., Smalley, D.M., et al. (2013). Application of multiplexed kinase

inhibitor beads to study kinome adaptations in drug-resistant leukemia. PLoS One *8*, e66755. 10.1371/journal.pone.0066755.

Coutadeur, S., Benyamine, H., Delalonde, L., de Oliveira, C., Leblond, B., Foucourt, A., Besson, T., Casagrande, A.S., Taverne, T., Girard, A., et al. (2015). A novel DYRK1A (dual specificity tyrosine phosphorylation-regulated kinase 1A) inhibitor for the treatment of Alzheimer's disease: effect on Tau and amyloid pathologies in vitro. Journal of neurochemistry *133*, 440-451. 10.1111/jnc.13018.

Dadon-Nachum, M., Melamed, E., and Offen, D. (2011). The "dying-back" phenomenon of motor neurons in ALS. Journal of molecular neuroscience : MN *43*, 470-477. 10.1007/s12031-010-9467-1.

Dauer, W., and Przedborski, S. (2003). Parkinson's disease: mechanisms and models. Neuron *39*, 889-909. 10.1016/s0896-6273(03)00568-3.

Davis, T.A., Loos, B., and Engelbrecht, A.M. (2015). Corrigendum to AHNAK: The giant jack of all trades [Cell. Signal. 26 (2014) 2683-2693]. Cellular signalling *27*, 187-188. 10.1016/j.cellsig.2014.10.004.

De Pascalis, C., and Etienne-Manneville, S. (2017). Single and collective cell migration: the mechanics of adhesions. Molecular biology of the cell *28*, 1833-1846. 10.1091/mbc.E17-03-0134.

Dekkers, M.P., Nikoletopoulou, V., and Barde, Y.A. (2013). Cell biology in neuroscience: Death of developing neurons: new insights and implications for connectivity. The Journal of cell biology *203*, 385-393. 10.1083/jcb.201306136.

Di Paolo, G., Antonsson, B., Kassel, D., Riederer, B.M., and Grenningloh, G. (1997). Phosphorylation regulates the microtubule-destabilizing activity of stathmin and its interaction with tubulin. FEBS letters *416*, 149-152. 10.1016/s0014-5793(97)01188-5.

Didonna, A., and Opal, P. (2019). The role of neurofilament aggregation in neurodegeneration: lessons from rare inherited neurological disorders. Molecular neurodegeneration *14*, 19. 10.1186/s13024-019-0318-4.

Dixit, R., Ross, J.L., Goldman, Y.E., and Holzbaur, E.L. (2008). Differential regulation of dynein and kinesin motor proteins by tau. Science *319*, 1086-1089. 10.1126/science.1152993.

Dong, J.M., Lau, L.S., Ng, Y.W., Lim, L., and Manser, E. (2009). Paxillin nuclear-cytoplasmic localization is regulated by phosphorylation of the LD4 motif: evidence that nuclear paxillin promotes cell proliferation. The Biochemical journal *418*, 173-184. 10.1042/BJ20080170.

DuBoff, B., Gotz, J., and Feany, M.B. (2012). Tau promotes neurodegeneration via DRP1 mislocalization in vivo. Neuron *75*, 618-632. 10.1016/j.neuron.2012.06.026.

Duncan, E.J., Lariviere, R., Bradshaw, T.Y., Longo, F., Sgarioto, N., Hayes, M.J., Romano, L.E.L., Nethisinghe, S., Giunti, P., Bruntraeger, M.B., et al. (2017a). Altered organisation of the intermediate filament cytoskeleton and relocalisation of proteostasis modulators in cells lacking the ataxia protein sacsin. Human molecular genetics. 10.1093/hmg/ddx197.

Duncan, E.J., Lariviere, R., Bradshaw, T.Y., Longo, F., Sgarioto, N., Hayes, M.J., Romano, L.E.L., Nethisinghe, S., Giunti, P., Bruntraeger, M.B., et al. (2017b). Altered organization of the intermediate filament cytoskeleton and relocalization of proteostasis modulators in cells lacking the ataxia protein sacsin. Human molecular genetics *26*, 3130-3143. 10.1093/hmg/ddx197.

Ebneth, A., Godemann, R., Stamer, K., Illenberger, S., Trinczek, B., and Mandelkow, E. (1998). Overexpression of tau protein inhibits kinesin-dependent trafficking of vesicles, mitochondria,

and endoplasmic reticulum: implications for Alzheimer's disease. The Journal of cell biology *143*, 777-794. 10.1083/jcb.143.3.777.

Engert, J.C., Berube, P., Mercier, J., Dore, C., Lepage, P., Ge, B., Bouchard, J.P., Mathieu, J., Melancon, S.B., Schalling, M., et al. (2000). ARSACS, a spastic ataxia common in northeastern Quebec, is caused by mutations in a new gene encoding an 11.5-kb ORF. Nat Genet *24*, 120-125. 10.1038/72769.

Ezratty, E.J., Partridge, M.A., and Gundersen, G.G. (2005). Microtubule-induced focal adhesion disassembly is mediated by dynamin and focal adhesion kinase. Nature cell biology *7*, 581-590. 10.1038/ncb1262.

Feng, T., Luan, L., Katz, II, Ullah, M., Van Deerlin, V.M., Trojanowski, J.Q., Lee, E.B., and Hu, F. (2022). TMEM106B deficiency impairs cerebellar myelination and synaptic integrity with Purkinje cell loss. Acta neuropathologica communications *10*, 33. 10.1186/s40478-022-01334-7.

Fink, J.K. (2013). Hereditary spastic paraplegia: clinico-pathologic features and emerging molecular mechanisms. Acta neuropathologica *126*, 307-328. 10.1007/s00401-013-1115-8.

Frederick, R.L., and Shaw, J.M. (2007). Moving mitochondria: establishing distribution of an essential organelle. Traffic *8*, 1668-1675. 10.1111/j.1600-0854.2007.00644.x.

Galea, G., and Simpson, J.C. (2015). High-content analysis of Rab protein function at the ER-Golgi interface. Bioarchitecture *5*, 44-53. 10.1080/19490992.2015.1102826.

Gan, L., Cookson, M.R., Petrucelli, L., and La Spada, A.R. (2018). Converging pathways in neurodegeneration, from genetics to mechanisms. Nature neuroscience *21*, 1300-1309. 10.1038/s41593-018-0237-7.

Gavriilidis, C., Laredj, L., Solinhac, R., Messaddeq, N., Viaud, J., Laporte, J., Sumara, I., and Hnia, K. (2018). The MTM1-UBQLN2-HSP complex mediates degradation of misfolded intermediate filaments in skeletal muscle. Nature cell biology *20*, 198-210. 10.1038/s41556-017-0024-9.

Genest, O., Wickner, S., and Doyle, S.M. (2019). Hsp90 and Hsp70 chaperones: Collaborators in protein remodeling. The Journal of biological chemistry *294*, 2109-2120. 10.1074/jbc.REV118.002806.

Gentil, B.J., Lai, G.T., Menade, M., Lariviere, R., Minotti, S., Gehring, K., Chapple, J.P., Brais, B., and Durham, H.D. (2019). Sacsin, mutated in the ataxia ARSACS, regulates intermediate filament assembly and dynamics. The FASEB journal : official publication of the Federation of American Societies for Experimental Biology *33*, 2982-2994. 10.1096/fj.201801556R.

Girard, M., Lariviere, R., Parfitt, D.A., Deane, E.C., Gaudet, R., Nossova, N., Blondeau, F., Prenosil, G., Vermeulen, E.G., Duchen, M.R., et al. (2012). Mitochondrial dysfunction and Purkinje cell loss in autosomal recessive spastic ataxia of Charlevoix-Saguenay (ARSACS). Proceedings of the National Academy of Sciences of the United States of America *109*, 1661-1666. 10.1073/pnas.1113166109.

Giustiniani, J., Daire, V., Cantaloube, I., Durand, G., Pous, C., Perdiz, D., and Baillet, A. (2009). Tubulin acetylation favors Hsp90 recruitment to microtubules and stimulates the signaling function of the Hsp90 clients Akt/PKB and p53. Cellular signalling *21*, 529-539. 10.1016/j.cellsig.2008.12.004.

Han, I., You, Y., Kordower, J.H., Brady, S.T., and Morfini, G.A. (2010). Differential vulnerability of neurons in Huntington's disease: the role of cell type-specific features. Journal of neurochemistry *113*, 1073-1091. 10.1111/j.1471-4159.2010.06672.x.

Heintz, T.G., Eva, R., and Fawcett, J.W. (2016). Regional Regulation of Purkinje Cell Dendritic Spines by Integrins and Eph/Ephrins. PLoS One *11*, e0158558. 10.1371/journal.pone.0158558.

Ikezu, S., Ingraham Dixie, K.L., Koro, L., Watanabe, T., Kaibuchi, K., and Ikezu, T. (2020). Tau-tubulin kinase 1 and amyloid-beta peptide induce phosphorylation of collapsin response mediator protein-2 and enhance neurite degeneration in Alzheimer disease mouse models. Acta neuropathologica communications *8*, 12. 10.1186/s40478-020-0890-4.

Ito, M. (2002). Historical review of the significance of the cerebellum and the role of Purkinje cells in motor learning. Annals of the New York Academy of Sciences *978*, 273-288. 10.1111/j.1749-6632.2002.tb07574.x.

Key, J., Harter, P.N., Sen, N.E., Gradhand, E., Auburger, G., and Gispert, S. (2020). Mid-Gestation lethality of Atxn2l-Ablated Mice. International journal of molecular sciences *21*. 10.3390/ijms21145124.

Kii, I., Nishiyama, T., and Kudo, A. (2016). Periostin promotes secretion of fibronectin from the endoplasmic reticulum. Biochemical and biophysical research communications *470*, 888-893. 10.1016/j.bbrc.2016.01.139.

Kilinc, D. (2018). The Emerging Role of Mechanics in Synapse Formation and Plasticity. Frontiers in cellular neuroscience *12*, 483. 10.3389/fncel.2018.00483.

Kiral, F.R., Kohrs, F.E., Jin, E.J., and Hiesinger, P.R. (2018). Rab GTPases and Membrane Trafficking in Neurodegeneration. Current biology : CB *28*, R471-R486. 10.1016/j.cub.2018.02.010.

Kishi, M., Pan, Y.A., Crump, J.G., and Sanes, J.R. (2005). Mammalian SAD kinases are required for neuronal polarization. Science *307*, 929-932. 10.1126/science.1107403.

Klionsky, D.J., Abdel-Aziz, A.K., Abdelfatah, S., Abdellatif, M., Abdoli, A., Abel, S., Abeliovich, H., Abildgaard, M.H., Abudu, Y.P., Acevedo-Arozena, A., et al. (2021). Guidelines for the use and interpretation of assays for monitoring autophagy (4th edition)(1). Autophagy *17*, 1-382. 10.1080/15548627.2020.1797280.

Krahn, A.I., Wells, C., Drewry, D.H., Beitel, L.K., Durcan, T.M., and Axtman, A.D. (2020). Defining the Neural Kinome: Strategies and Opportunities for Small Molecule Drug Discovery to Target Neurodegenerative Diseases. ACS Chem Neurosci *11*, 1871-1886. 10.1021/acschemneuro.0c00176.

Kvarnung, M., Shahsavani, M., Taylan, F., Moslem, M., Breeuwsma, N., Laan, L., Schuster, J., Jin, Z., Nilsson, D., Lieden, A., et al. (2019). Ataxia in Patients With Bi-Allelic NFASC Mutations and Absence of Full-Length NF186. Frontiers in genetics *10*, 896. 10.3389/fgene.2019.00896.

Lackie, R.E., Maciejewski, A., Ostapchenko, V.G., Marques-Lopes, J., Choy, W.Y., Duennwald, M.L., Prado, V.F., and Prado, M.A.M. (2017). The Hsp70/Hsp90 Chaperone Machinery in Neurodegenerative Diseases. Frontiers in neuroscience *11*, 254. 10.3389/fnins.2017.00254.

Lariviere, R., Gaudet, R., Gentil, B.J., Girard, M., Conte, T.C., Minotti, S., Leclerc-Desaulniers, K., Gehring, K., McKinney, R.A., Shoubridge, E.A., et al. (2015). Sacs knockout mice present pathophysiological defects underlying autosomal recessive spastic ataxia of Charlevoix-Saguenay. Human molecular genetics *24*, 727-739. 10.1093/hmg/ddu491.

Lariviere, R., Sgarioto, N., Marquez, B.T., Gaudet, R., Choquet, K., McKinney, R.A., Watt, A.J., and Brais, B. (2019). Sacs R272C missense homozygous mice develop an ataxia phenotype. Molecular brain *12*, 19. 10.1186/s13041-019-0438-3.

673 Leube, R.E., Moch, M., and Windoffer, R. (2015). Intermediate filaments and the regulation of
674 focal adhesion. Curr Opin Cell Biol *32*, 13-20. 10.1016/j.ceb.2014.09.011.

675 Lopes, S., Teplytska, L., Vaz-Silva, J., Dioli, C., Trindade, R., Morais, M., Webhofer, C.,
676 Maccarrone, G., Almeida, O.F.X., Turck, C.W., et al. (2017). Tau Deletion Prevents Stress-
677 Induced Dendritic Atrophy in Prefrontal Cortex: Role of Synaptic Mitochondria. Cereb Cortex *27*,
678 2580-2591. 10.1093/cercor/bhw057.

679 Manczak, M., and Reddy, P.H. (2012). Abnormal interaction between the mitochondrial fission
680 protein Drp1 and hyperphosphorylated tau in Alzheimer's disease neurons: implications for
681 mitochondrial dysfunction and neuronal damage. Human molecular genetics *21*, 2538-2547.
682 10.1093/hmg/dds072.

683 Martin, M., and Akhmanova, A. (2018). Coming into Focus: Mechanisms of Microtubule Minus-
684 End Organization. Trends in cell biology *28*, 574-588. 10.1016/j.tcb.2018.02.011.

685 Martin, M.H., Bouchard, J.P., Sylvain, M., St-Onge, O., and Truchon, S. (2007). Autosomal
686 recessive spastic ataxia of Charlevoix-Saguenay: a report of MR imaging in 5 patients. AJNR.
687 American journal of neuroradiology *28*, 1606-1608. 10.3174/ajnr.A0603.

688 McClellan, A.J., Xia, Y., Deutschbauer, A.M., Davis, R.W., Gerstein, M., and Frydman, J.
689 (2007). Diverse cellular functions of the Hsp90 molecular chaperone uncovered using systems
690 approaches. Cell *131*, 121-135. 10.1016/j.cell.2007.07.036.

691 Melkov, A., and Abdu, U. (2018). Regulation of long-distance transport of mitochondria along
692 microtubules. Cellular and molecular life sciences : CMLS *75*, 163-176. 10.1007/s00018-017-
693 2590-1.

694 Morani, F., Doccini, S., Chiorino, G., Fattori, F., Galatolo, D., Sciarrillo, E., Gemignani, F.,
695 Zuchner, S., Bertini, E.S., and Santorelli, F.M. (2020). Functional Network Profiles in ARSACS
696 Disclosed by Aptamer-Based Proteomic Technology. Front Neurol *11*, 603774.
697 10.3389/fneur.2020.603774.

698 Moreno-Layseca, P., Icha, J., Hamidi, H., and Ivaska, J. (2019). Integrin trafficking in cells and
699 tissues. Nature cell biology *21*, 122-132. 10.1038/s41556-018-0223-z.

700 Morfini, G.A., Burns, M., Binder, L.I., Kanaan, N.M., LaPointe, N., Bosco, D.A., Brown, R.H., Jr.,
701 Brown, H., Tiwari, A., Hayward, L., et al. (2009). Axonal transport defects in neurodegenerative
702 diseases. The Journal of neuroscience : the official journal of the Society for Neuroscience *29*,
703 12776-12786. 10.1523/JNEUROSCI.3463-09.2009.

704 Murase, S., and Hayashi, Y. (1998). Integrin alpha1 localization in murine central and peripheral
705 nervous system. The Journal of comparative neurology *395*, 161-176. 10.1002/(sici)1096-
706 9861(19980601)395:2<161::aid-cne2>3.0.co;2-0.

707 Naguib, A., Bencze, G., Cho, H., Zheng, W., Tocilj, A., Elkayam, E., Faehnle, C.R., Jaber, N.,
708 Pratt, C.P., Chen, M., et al. (2015). PTEN functions by recruitment to cytoplasmic vesicles. Mol
709 Cell *58*, 255-268. 10.1016/j.molcel.2015.03.011.

710 Ng, D.H., Humphries, J.D., Byron, A., Millon-Fremillon, A., and Humphries, M.J. (2014).
711 Microtubule-dependent modulation of adhesion complex composition. PLoS One *9*, e115213.
712 10.1371/journal.pone.0115213.

713 Nieuwenhuis, B., Haenzi, B., Andrews, M.R., Verhaagen, J., and Fawcett, J.W. (2018). Integrins
714 promote axonal regeneration after injury of the nervous system. Biological reviews of the
715 Cambridge Philosophical Society *93*, 1339-1362. 10.1111/brv.12398.

716 Noordstra, I., and Akhmanova, A. (2017). Linking cortical microtubule attachment and
717 exocytosis. F1000Res *6*, 469. 10.12688/f1000research.10729.1.

718 Nunomura, K., Nagano, K., Itagaki, C., Taoka, M., Okamura, N., Yamauchi, Y., Sugano, S.,
719 Takahashi, N., Izumi, T., and Isobe, T. (2005). Cell surface labeling and mass spectrometry
720 reveal diversity of cell surface markers and signaling molecules expressed in undifferentiated
721 mouse embryonic stem cells. Mol Cell Proteomics *4*, 1968-1976. 10.1074/mcp.M500216-
722 MCP200.

723 Ochoa, D., Jarnuczak, A.F., Vieitez, C., Gehre, M., Soucheray, M., Mateus, A., Kleefeldt, A.A.,
724 Hill, A., Garcia-Alonso, L., Stein, F., et al. (2020). The functional landscape of the human
725 phosphoproteome. Nature biotechnology *38*, 365-373. 10.1038/s41587-019-0344-3.

726 Pan, C., Chun, J., Li, D., Boese, A.C., Li, J., Kang, J., Umano, A., Jiang, Y., Song, L.,
727 Magliocca, K.R., et al. (2019). Hsp90B enhances MAST1-mediated cisplatin resistance by
728 protecting MAST1 from proteosomal degradation. The Journal of clinical investigation *129*,
729 4110-4123. 10.1172/JCI125963.

730 Parfitt, D.A., Michael, G.J., Vermeulen, E.G., Prodromou, N.V., Webb, T.R., Gallo, J.M.,
731 Cheetham, M.E., Nicoll, W.S., Blatch, G.L., and Chapple, J.P. (2009). The ataxia protein sacsin
732 is a functional co-chaperone that protects against polyglutamine-expanded ataxin-1. Human
733 molecular genetics *18*, 1556-1565. 10.1093/hmg/ddp067.

734 Park, Y.K., and Goda, Y. (2016). Integrins in synapse regulation. Nature reviews. Neuroscience
735 *17*, 745-756. 10.1038/nrn.2016.138.

736 Pollerberg, G.E., Thelen, K., Theiss, M.O., and Hochlehnert, B.C. (2013). The role of cell
737 adhesion molecules for navigating axons: density matters. Mechanisms of development *130*,
738 359-372. 10.1016/j.mod.2012.11.002.

739 Quinta, H.R., Galigniana, N.M., Erlejman, A.G., Lagadari, M., Piwien-Pilipuk, G., and
740 Galigniana, M.D. (2011). Management of cytoskeleton architecture by molecular chaperones
741 and immunophilins. Cellular signalling *23*, 1907-1920. 10.1016/j.cellsig.2011.07.023.

742 Raff, M.C., Whitmore, A.V., and Finn, J.T. (2002). Axonal self-destruction and
743 neurodegeneration. Science *296*, 868-871. 10.1126/science.1068613.

744 Reddy, P.H. (2011). Abnormal tau, mitochondrial dysfunction, impaired axonal transport of
745 mitochondria, and synaptic deprivation in Alzheimer's disease. Brain research *1415*, 136-148.
746 10.1016/j.brainres.2011.07.052.

747 Rico, B., Beggs, H.E., Schahin-Reed, D., Kimes, N., Schmidt, A., and Reichardt, L.F. (2004).
748 Control of axonal branching and synapse formation by focal adhesion kinase. Nature
749 neuroscience *7*, 1059-1069. 10.1038/nn1317.

750 Robertson, L.K., and Ostergaard, H.L. (2011). Paxillin associates with the microtubule
751 cytoskeleton and the immunological synapse of CTL through its leucine-aspartic acid domains
752 and contributes to microtubule organizing center reorientation. J Immunol *187*, 5824-5833.
753 10.4049/jimmunol.1003690.

754 Sakurai, T., Lustig, M., Babiarz, J., Furley, A.J., Tait, S., Brophy, P.J., Brown, S.A., Brown, L.Y.,
755 Mason, C.A., and Grumet, M. (2001). Overlapping functions of the cell adhesion molecules Nr-
756 CAM and L1 in cerebellar granule cell development. The Journal of cell biology *154*, 1259-1273.
757 10.1083/jcb.200104122.

758 Salvadores, N., Sanhueza, M., Manque, P., and Court, F.A. (2017). Axonal Degeneration during
759 Aging and Its Functional Role in Neurodegenerative Disorders. Frontiers in neuroscience *11*,
760 451. 10.3389/fnins.2017.00451.

761 Samarzija, I., Dekanic, A., Humphries, J.D., Paradzik, M., Stojanovic, N., Humphries, M.J., and
762 Ambriovic-Ristov, A. (2020). Integrin Crosstalk Contributes to the Complexity of Signalling and
763 Unpredictable Cancer Cell Fates. Cancers *12*. 10.3390/cancers12071910.

764 Sathyamurthy, A., Barik, A., Dobrott, C.I., Matson, K.J.E., Stoica, S., Pursley, R., Chesler, A.T.,
765 and Levine, A.J. (2020). Cerebellospinal Neurons Regulate Motor Performance and Motor
766 Learning. Cell reports *31*, 107595. 10.1016/j.celrep.2020.107595.

767 Saunders, A., Macosko, E.Z., Wysoker, A., Goldman, M., Krienen, F.M., de Rivera, H., Bien, E.,
768 Baum, M., Bortolin, L., Wang, S., et al. (2018). Molecular Diversity and Specializations among
769 the Cells of the Adult Mouse Brain. Cell *174*, 1015-1030 e1016. 10.1016/j.cell.2018.07.028.

770 Seetharaman, S., and Etienne-Manneville, S. (2019). Microtubules at focal adhesions - a
771 double-edged sword. Journal of cell science *132*. 10.1242/jcs.232843.

772 Sengupta, A., Kabat, J., Novak, M., Wu, Q., Grundke-Iqbal, I., and Iqbal, K. (1998).
773 Phosphorylation of tau at both Thr 231 and Ser 262 is required for maximal inhibition of its
774 binding to microtubules. Archives of biochemistry and biophysics *357*, 299-309.
775 10.1006/abbi.1998.0813.

776 Shinde, S.R., and Maddika, S. (2016). PTEN modulates EGFR late endocytic trafficking and
777 degradation by dephosphorylating Rab7. Nature communications *7*, 10689.
778 10.1038/ncomms10689.

779 Shipley, M.M., Mangold, C.A., and Szpara, M.L. (2016). Differentiation of the SH-SY5Y Human
780 Neuroblastoma Cell Line. Journal of visualized experiments : JoVE, 53193. 10.3791/53193.

781 Sistani, L., Rodriguez, P.Q., Hultenby, K., Uhlen, M., Betsholtz, C., Jalanko, H., Tryggvason, K.,
782 Wernerson, A., and Patrakka, J. (2013). Neuronal proteins are novel components of podocyte
783 major processes and their expression in glomerular crescents supports their role in crescent
784 formation. Kidney international *83*, 63-71. 10.1038/ki.2012.321.

785 Smigiel, R., Sherman, D.L., Rydzanicz, M., Walczak, A., Mikolajkow, D., Krolak-Olejnik, B.,
786 Kosinska, J., Gasperowicz, P., Biernacka, A., Stawinski, P., et al. (2018). Homozygous mutation
787 in the Neurofascin gene affecting the glial isoform of Neurofascin causes severe
788 neurodevelopment disorder with hypotonia, amimia and areflexia. Human molecular genetics
789 *27*, 3669-3674. 10.1093/hmg/ddy277.

790 Snider, N.T., and Omary, M.B. (2014). Post-translational modifications of intermediate filament
791 proteins: mechanisms and functions. Nature reviews. Molecular cell biology *15*, 163-177.
792 10.1038/nrm3753.

793 Stanga, S., Caretto, A., Boido, M., and Vercelli, A. (2020). Mitochondrial Dysfunctions: A Red
794 Thread across Neurodegenerative Diseases. International journal of molecular sciences *21*.
795 10.3390/ijms21103719.

796 Stoothoff, W.H., and Johnson, G.V. (2005). Tau phosphorylation: physiological and pathological
797 consequences. Biochimica et biophysica acta *1739*, 280-297. 10.1016/j.bbadis.2004.06.017.

798 Sulzmaier, F.J., Jean, C., and Schlaepfer, D.D. (2014). FAK in cancer: mechanistic findings and
799 clinical applications. Nat Rev Cancer *14*, 598-610. 10.1038/nrc3792.

800 Suresh Babu, S., Wojtowicz, A., Freichel, M., Birnbaumer, L., Hecker, M., and Cattaruzza, M.
801 (2012). Mechanism of stretch-induced activation of the mechanotransducer zyxin in vascular
802 cells. Science signaling *5*, ra91. 10.1126/scisignal.2003173.

803 Synofzik, M., Soehn, A.S., Gburek-Augustat, J., Schicks, J., Karle, K.N., Schule, R., Haack,
804 T.B., Schoning, M., Biskup, S., Rudnik-Schoneborn, S., et al. (2013). Autosomal recessive

spastic ataxia of Charlevoix Saguenay (ARSACS): expanding the genetic, clinical and imaging spectrum. Orphanet journal of rare diseases *8*, 41. 10.1186/1750-1172-8-41.

Szklarczyk, D., Gable, A.L., Lyon, D., Junge, A., Wyder, S., Huerta-Cepas, J., Simonovic, M., Doncheva, N.T., Morris, J.H., Bork, P., et al. (2019). STRING v11: protein-protein association networks with increased coverage, supporting functional discovery in genome-wide experimental datasets. Nucleic acids research *47*, D607-D613. 10.1093/nar/gky1131.

Takano, T., Wallace, J.T., Baldwin, K.T., Purkey, A.M., Uezu, A., Courtland, J.L., Soderblom, E.J., Shimogori, T., Maness, P.F., Eroglu, C., and Soderling, S.H. (2020). Chemico-genetic discovery of astrocytic control of inhibition in vivo. Nature *588*, 296-302. 10.1038/s41586-020-2926-0.

Tamura, M., Gu, J., Takino, T., and Yamada, K.M. (1999). Tumor suppressor PTEN inhibition of cell invasion, migration, and growth: differential involvement of focal adhesion kinase and p130Cas. Cancer research *59*, 442-449.

Tang, Y., Tao, Y., Wang, L., Yang, L., Jing, Y., Jiang, X., Lei, L., Yang, Z., Wang, X., Peng, M., et al. (2021). NPM1 mutant maintains ULK1 protein stability via TRAF6-dependent ubiquitination to promote autophagic cell survival in leukemia. The FASEB journal : official publication of the Federation of American Societies for Experimental Biology *35*, e21192. 10.1096/fj.201903183RRR.

Trogden, K.P., Battaglia, R.A., Kabiraj, P., Madden, V.J., Herrmann, H., and Snider, N.T. (2018). An image-based small-molecule screen identifies vimentin as a pharmacologically relevant target of simvastatin in cancer cells. The FASEB journal : official publication of the Federation of American Societies for Experimental Biology *32*, 2841-2854. 10.1096/fj.201700663R.

Valiente, M., Andres-Pons, A., Gomar, B., Torres, J., Gil, A., Tapparel, C., Antonarakis, S.E., and Pulido, R. (2005). Binding of PTEN to specific PDZ domains contributes to PTEN protein stability and phosphorylation by microtubule-associated serine/threonine kinases. The Journal of biological chemistry *280*, 28936-28943. 10.1074/jbc.M504761200.

Vermeer, S., van de Warrenburg, B.P., Kamsteeg, E.J., Brais, B., and Synofzik, M. (1993). Arsacs. In GeneReviews((R)), M.P. Adam, H.H. Ardinger, R.A. Pagon, S.E. Wallace, L.J.H. Bean, G. Mirzaa, and A. Amemiya, eds.

Walter, J.T., Alvina, K., Womack, M.D., Chevez, C., and Khodakhah, K. (2006). Decreases in the precision of Purkinje cell pacemaking cause cerebellar dysfunction and ataxia. Nature neuroscience *9*, 389-397. 10.1038/nn1648.

Wu, Y., Ding, Y., Zheng, X., and Liao, K. (2020). The molecular chaperone Hsp90 maintains Golgi organization and vesicular trafficking by regulating microtubule stability. Journal of molecular cell biology *12*, 448-461. 10.1093/jmcb/mjz093.

Xicoy, H., Wieringa, B., and Martens, G.J. (2017). The SH-SY5Y cell line in Parkinson's disease research: a systematic review. Molecular neurodegeneration *12*, 10. 10.1186/s13024-017-0149-0.

Xiong, X., Wang, Y., Liu, C., Lu, Q., Liu, T., Chen, G., Rao, H., and Luo, S. (2014). Heat shock protein 90beta stabilizes focal adhesion kinase and enhances cell migration and invasion in breast cancer cells. Experimental cell research *326*, 78-89. 10.1016/j.yexcr.2014.05.018.

Zhao, X., and Guan, J.L. (2011). Focal adhesion kinase and its signaling pathways in cell migration and angiogenesis. Advanced drug delivery reviews *63*, 610-615. 10.1016/j.addr.2010.11.001.

Zhou, C., Cunningham, L., Marcus, A.I., Li, Y., and Kahn, R.A. (2006). Arl2 and Arl3 regulate different microtubule-dependent processes. Molecular biology of the cell *17*, 2476-2487. 10.1091/mbc.e05-10-0929.

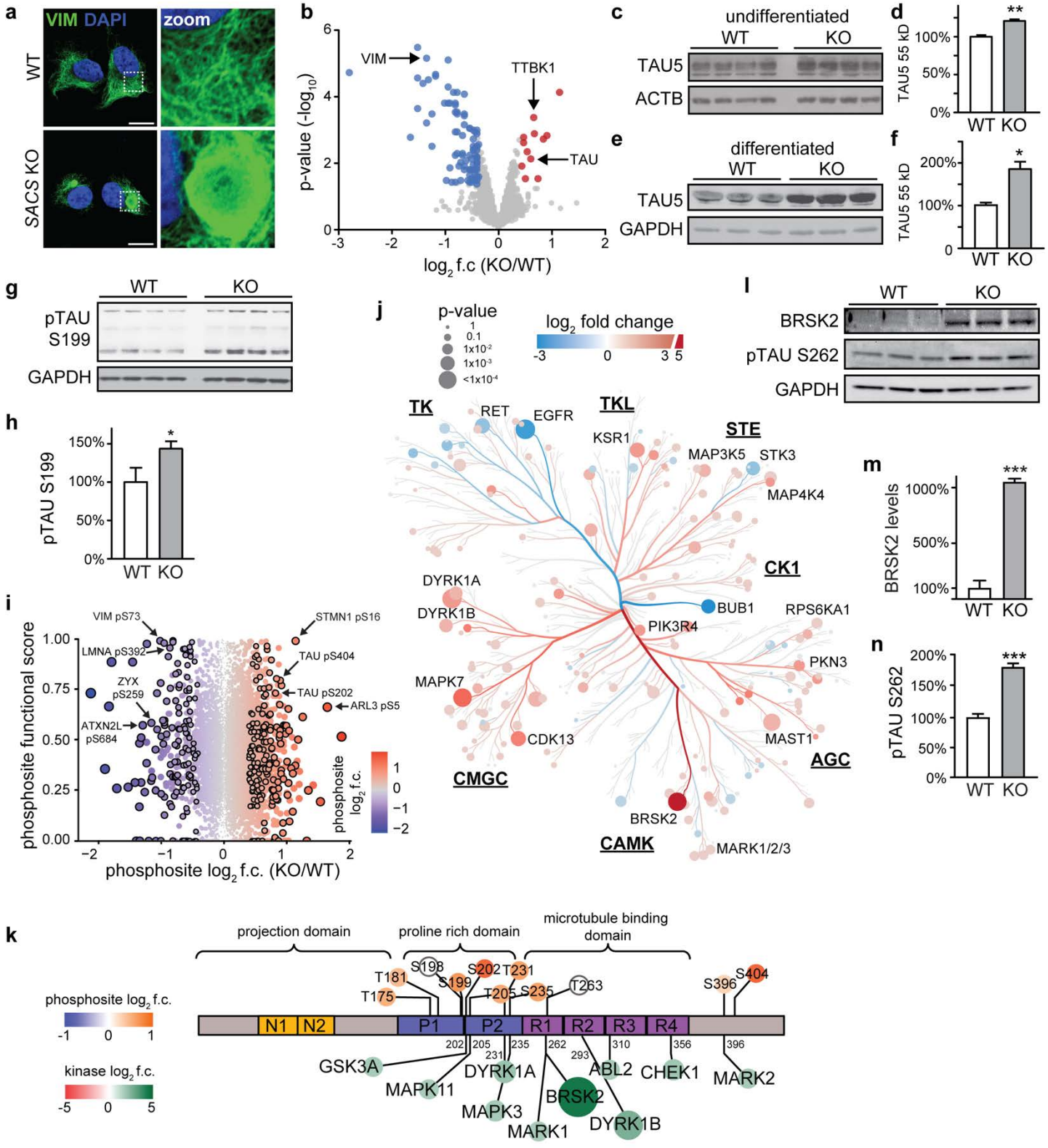

Figure 1 – Proteomic profiling of sacsin KO cells

a. Representative confocal images of control (WT) and sacsin knockout (KO) SH-SY5Y neuroblastoma cells immunostained for the intermediate filament protein vimentin. Scale bar = 10 μm.

b. Global proteomic profiling of sacsin KO SH-SY5Y cells. Cutoffs for significance were $p<0.05$ and $\log_2$ fold change (f.c.) -/+0.4.

c-f. Western Blot analysis quantification of pan-tau (Tau5) in sacsin KO and WT cells in undifferentiated (c,d) and neuronally differentiated (e,f) SH-SY5Y cells.

g,h. Western blot and quantification of phosphorylated tau at serine 199.

i. Functional analysis of altered phosphosites in sacsin KO cells. Y-axis is the functional score assigned by Ochoa et al (2020), which combines 59 features to assess the impact of each phosphosite on organismal fitness. A higher score reflects increased predicted effect on fitness. Dot color and size reflect $\log_2$ f.c. Black outlines label phosphosites with $p<0.05$ and $\log_2$ f.c. -/+0.4.

j. Phylogenetic tree of the kinome in sacsin KO cells. Color indicates $\log_2$ f.c. of kinase abundance, size indicates $-\log_{10}$ p-value. Underlined abbreviations refer to phylogenetically related kinase families.

k. Protein map of tau isoform 2 (2N4R). Phosphosites identified in phosphoproteomic profiling are labelled above diagram. Tau kinases identified in the kinome profiling are listed below, labeled with known phosphosites. Colored circles correlate with $\log_2$ f.c. of significantly differentially expressed phosphosites or kinases.

l-n. Western blot and quantification for BRSK2, and the BRSK2 target residue pTAU S262.

Unless otherwise noted, all error bars are S.E.M., all statistical tests are Student's t-test (*P<0.05, **P<0.01, ***P<0.001, ****P<0.0001).

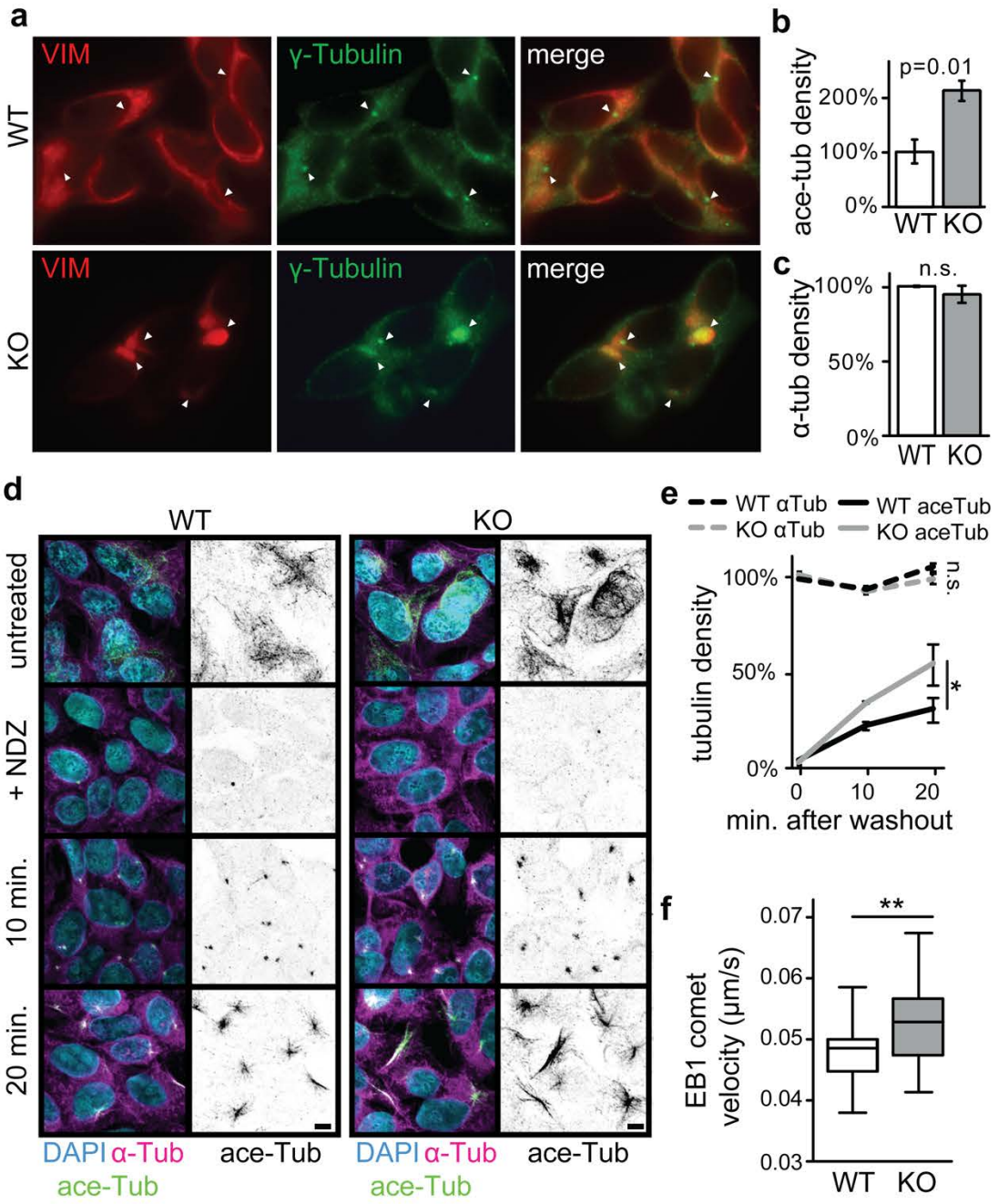

Figure 2 – Altered microtubule structure and dynamics in sacsin KO cells

a. Confocal immunofluorescent images of sacsin WT/KO cells stained for vimentin, and the MTOC marker gamma tubulin. Arrowheads point to the most intense signal in each cell, showing that vimentin bundles surround the MTOC in sacsin KO cells. Scale bar = 10 μm.

b,c. Quantification of images in Extended Data Fig. 2b, showing altered microtubule acetylation in sacsin KO cells (b) without global changes in microtubule structure (c).

d. Confocal images of WT/KO cells treated with nocodazole (NDZ) labeled for alpha- and acetylated-tubulin at indicated time points following nocodazole washout. Note the faster microtubule repolymerization and acetylation in sacsin KO cells. Scale bar = 10 μm.

e. Quantification of images in (d). n = 3 coverslips; One-way ANOVA with Tukey post-test.

f. Quantification of microtubule polymerization velocity marked by EB1-GFP movement in WT/KO cells on TIRF microscope from Supplemental Video 1. n=34 WT and n=25 sacsin KO cells, examined from at least three independent experiments; unpaired t-test.

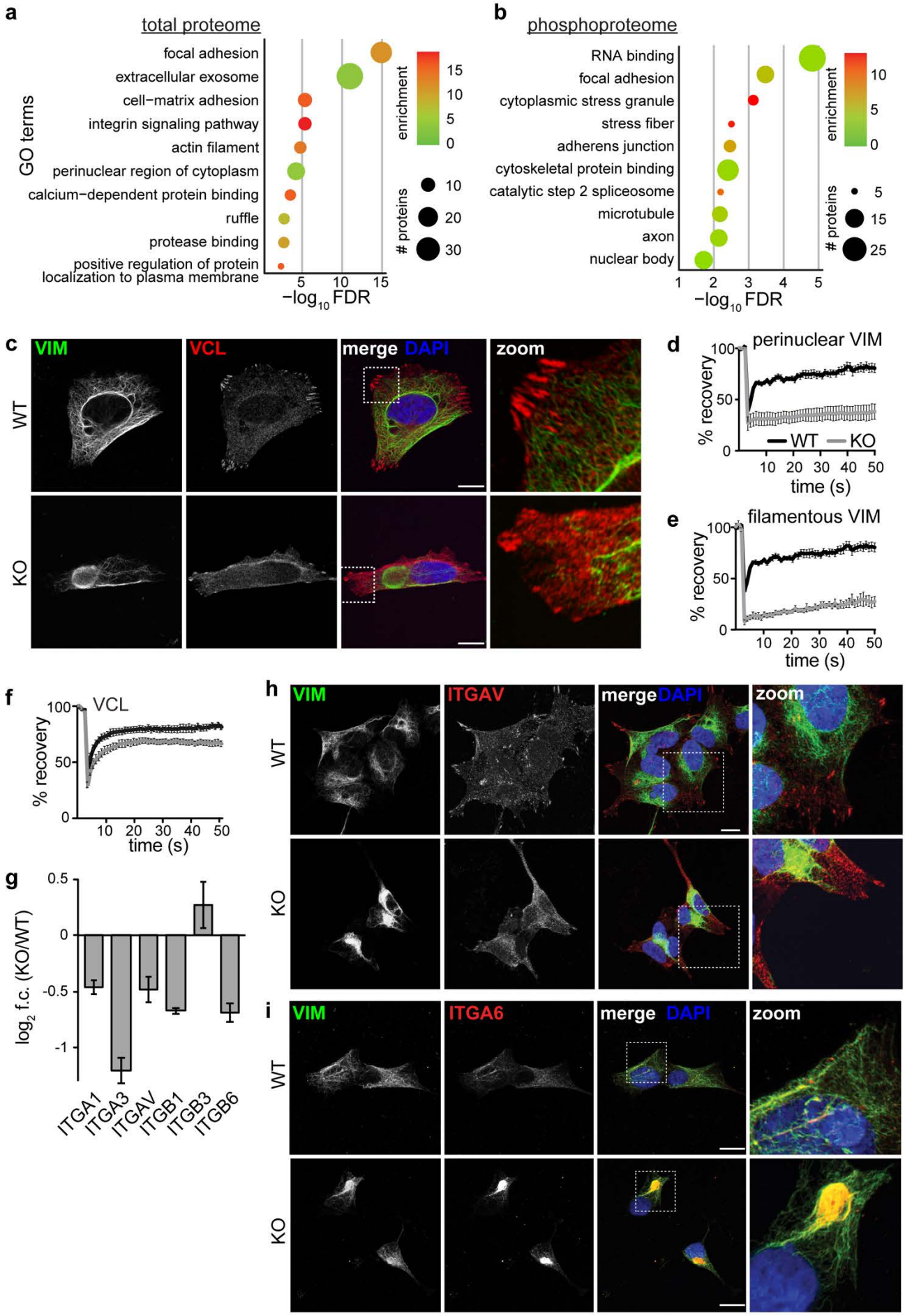
a
total proteome
GO terms
focal adhesion
extracellular exosome
cell−matrix adhesion
integrin signaling pathway
actin filament
perinuclear region of cytoplasm
calcium−dependent protein binding
ruffle
protease binding
positive regulation of protein localization to plasma membrane
−log10 FDR
enrichment
proteins
b
phosphoproteome
RNA binding
focal adhesion
cytoplasmic stress granule
stress fiber
adherens junction
cytoskeletal protein binding
catalytic step 2 spliceosome
microtubule
axon
nuclear body
c
VIM
VCL
merge DAPI
zoom
WT
KO
d
perinuclear VIM
% recovery
WT
KO
time (s)
e
filamentous VIM
f
VCL
g
log2 f.c. (KO/WT)
ITGA1
ITGA3
ITGAV
ITGB1
ITGB3
ITGB6
h
VIM
ITGAV
merge DAPI
zoom
i
VIM
ITGA6
merge DAPI
zoom

Figure 3 – Focal Adhesions are altered in sacsin KO cells

a. GO term analysis from the total proteome ($p<0.05$, $\log_2$ f.c. cutoff -/+0.4),
b. GO term analysis for phosphoproteins with $p<0.05$, $\log_2$ f.c. <-0.4, and abs($\log_2$ f.c. phosphoproteome – $\log_2$ f.c. total proteome) > 0.5. (from Fig. S1g, Supplemental Table 1).
c. Confocal images of WT/KO SH-SY5Y cells immunolabeled for vimentin and the focal adhesion protein vinculin.

d-f. FRAP analysis of perinuclear vimentin (d), filamentous vimentin on the periphery of the cell away from vimentin bundle (e), and the focal adhesion protein vinculin (f). Cells were transfected with EGFP-VIM or tomato-VCL expression vectors and defined 2 × 2 µm regions of interest were bleached by using a 488-nm or 568-nm laser line. Recovery was monitored over 50 cycles of imaging with a 1-s interval. n=10 cells from each of three independent experiments.

g. Changes in levels of integrin proteins quantified by mass-spectrometry (Fig. 1b).

h,i. Representative confocal images of cells immunolabeled for ITGAV (h) and ITGA6 (i). Scale bar = 10 µm.

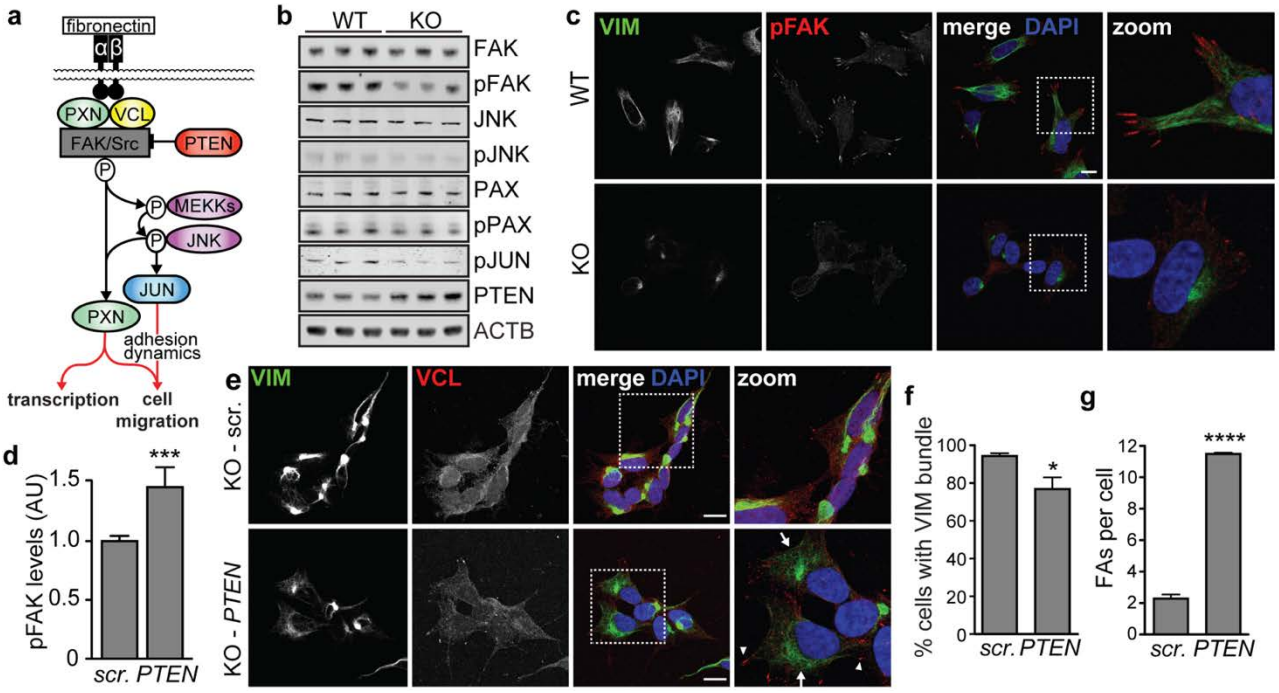

Figure 4 – Targeting upstream focal adhesion regulator PTEN rescues focal adhesion and vimentin bundling phenotypes in sacsin KO cells.

a. Model of regulators and effectors of focal adhesion signaling

b. Western blots for regulators PTEN, FAK, phosphorylated FAK (pFAK-Tyr397), JNK, phosphorylated JNK (pJNK), paxillin (PAX), phosphorylated paxillin (pPAX) and phosphorylated Jun (pJUN) in total cell lysates from sacsin KO and control cells. β-actin used to confirm equivalent sample loading.

c. Representative confocal images of cells immunolabeled for pFAK. Scale bar = 10 μm.

d. pFAK levels with sacsin KO cells treated with either scrambled (scr.) or siRNA targeting *PTEN.*

e. Representative confocal images for cells transfected with siRNAs targeting PTEN (*PTEN*) or scramble siRNAs and immunolabeled for vimentin and vinculin. Arrowheads in the zoomed panel indicate cells with prominent focal adhesions, arrows indicate cells with absent or reduced perinuclear accumulations of vimentin. Scale bars = 10 μm.

f,g. Quantification of the incidence of sacsin KO cells with perinuclear accumulations of vimentin (f) or vinculin positive focal adhesions (g) 48 hours after transfection with siRNAs targeting *PTEN* or scr. siRNAs. n=3 replicates with >100 cells in each replicate.

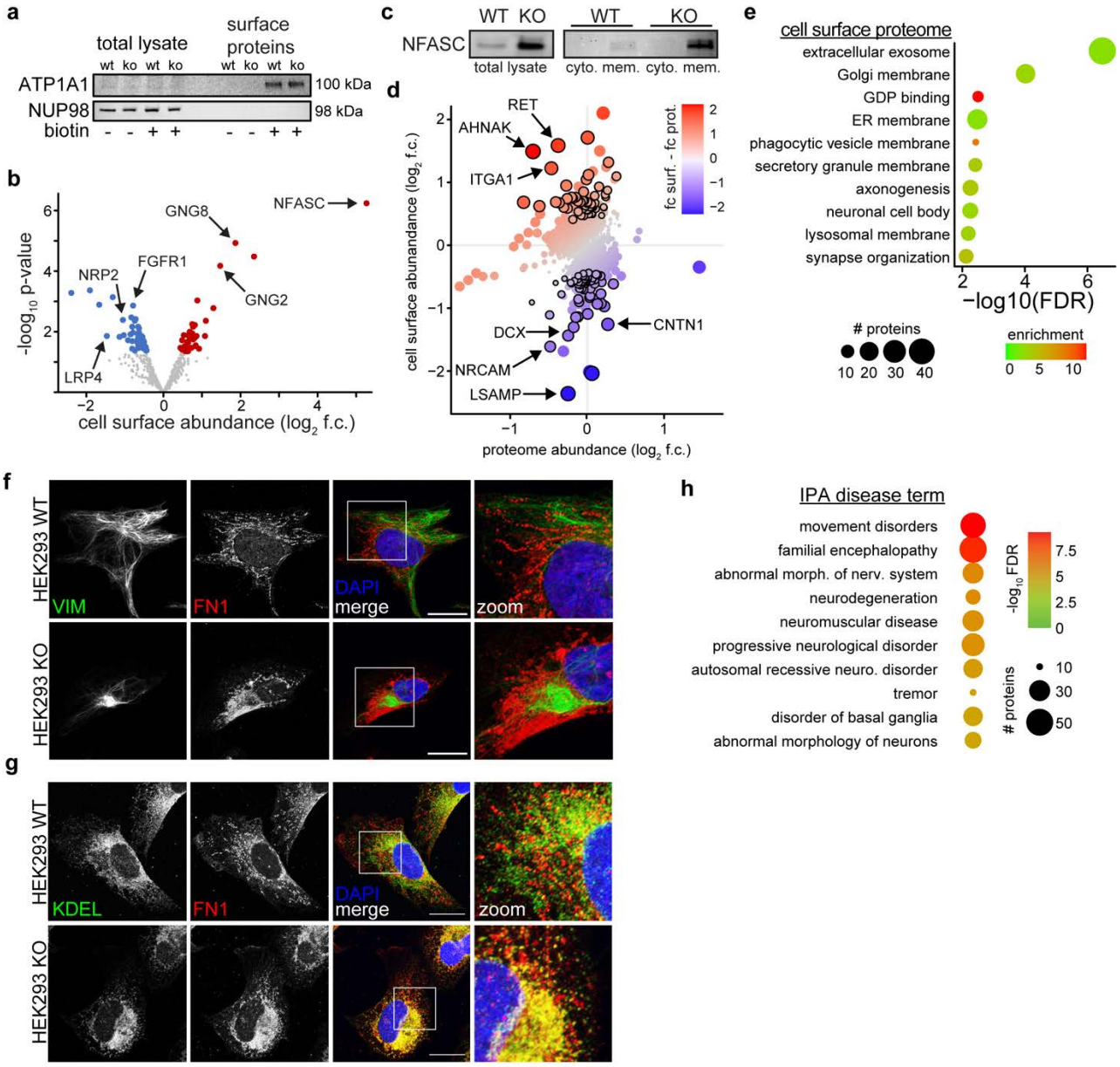

Figure 5 – The loss of sacsin affects the localization of cell adhesion proteins

a. Western blot of membrane purification approach, illustrated by ATP1A1, a membrane bound Na/K ATPase, and NUP98, a nuclear pore protein. In total lysate only NUP98 is detectable. After purification ATP1A1 is detectable only in conditions that were treated with biotin, and NUP98 is not longer detected, suggested labelling specificity and enrichment of cell surface proteins.

b. Volcano plot of cell surface proteins only detected in surface proteomic experiment.

c. Western blot of NFASC in total lysate (left), and fractionated cytoplasmic or membrane fractions in WT and sacsin KO cells.

d. Levels of proteins detected in both cell surface and proteomic datasets. Proteins are colored by the disparity between these two datasets (f.c. surface – f.c. proteome), with red indicating more, and blue less membrane abundance relative to total protein levels. Black outlines are proteins with $p<0.05$, $\log_2$ f.c. -/+ 0.4 in the surfaceome dataset.

e. GO term analysis of proteins differentially localized in membrane of sacsin KO cells ($p<0.05$, $\log_2$ f.c. -/+ 0.4).

f,g. Representative confocal images for fibronectin (levels not affected in any proteomic experiment) and vimentin (f) and ER marker KDEL (g) in WT and sacsin KO HEK293 cells. Scale bar = 10 µm.

h. Disease enrichment analysis with Ingenuity Pathway Analysis (IPA) of significantly differentially expressed cell-surface proteins ($p<0.05$, $\log_2$ f.c. -/+ 0.4).

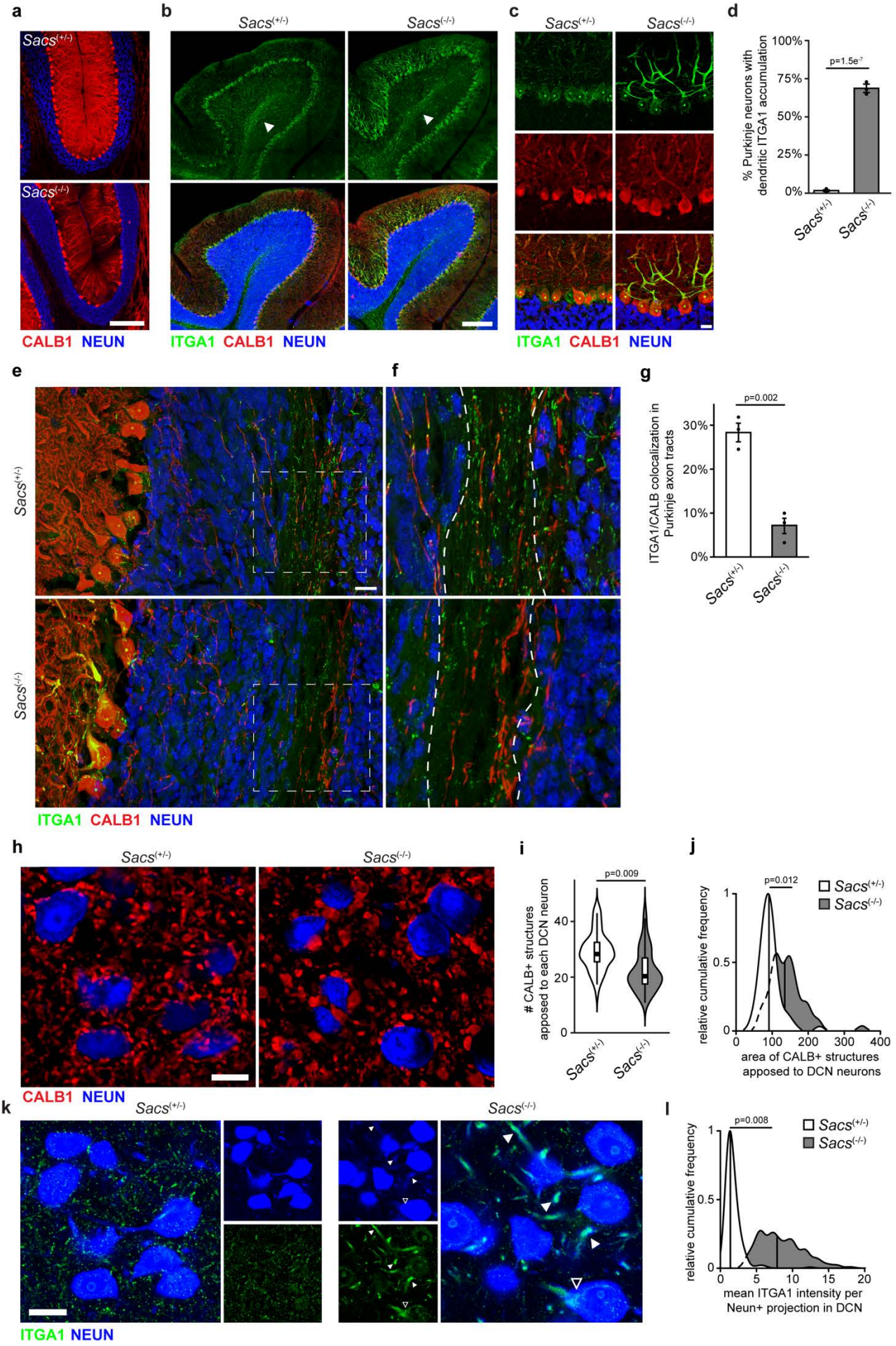
a
b
c
d
Sacs(+/-)
Sacs(-/-)
CALB1 NEUN
ITGA1 CALB1 NEUN
% Purkinje neurons with dendritic ITGA1 accumulation
100%
75%
50%
25%
0%
p=1.5e-7
e
f
g
ITGA1/CALB colocalization in Purkinje axon tracts
30%
20%
10%
0%
p=0.002
h
i
j
CALB+ structures apposed to each DCN neuron
40
20
0
p=0.009
relative cumulative frequency
1
0.5
0
p=0.012
0
100
200
300
400
area of CALB+ structures apposed to DCN neurons
k
l
mean ITGA1 intensity per Neun+ projection in DCN
0
5
10
15
20
p=0.008

Figure 6 – Altered localization of membrane proteins and synapses in ARSACS mice

a. Confocal imaging of Purkinje neurons in litter mate controlled P120 *SACS*$^{(+/-)}$ and *SACS*$^{(-/-)}$ mice, demonstrating substantial Purkinje cell loss. Purkinje marker calbindin-D28K (CALB1), and neuronal marker (NEUN). *Sacs*$^{(+/-)}$ mice are phenotypically normal, analogous to unaffected human carriers. Scale bar = 200 µm.

b. Representative confocal image of cerebellum in P60 mice, stained for integrin A1 (ITGA1), one of the most significantly mislocalized proteins in sacsin KO cells (Fig. 5d). Arrowheads denote prominent ITGA1 staining in white matter axonal tracts. Scale bar = 200 µm

c. High magnification of ITGA1 staining in the Purkinje neuron layer in P60 mice. Scale bar = 20 µm.

d. Quantification of ITGA1 accumulation in cerebellar sagittal sections. Abnormal accumulation was defined as mean ITGA1 intensity in dendritic arbor greater than 3 standard deviations above the mean in *Sacs*$^{(+/-)}$ mice. A replicate is defined as a sex matched het/KO animals from the same litter. Average of two sections per animal, ~240 Purkinje counted neurons per section. n=3 litters. Paired t-test (litter as pairing variable.

e. Representative confocal image of Purkinje axon tracts through the NEUN+ granule cell layer, and NEUN- white matter tracts in P60 mice. Scale bar = 20 µm.

f. Zoomed in region from Fig. 6e, a single z-plane. Dashed lines mark white matter axonal tracts for quantification in Fig. 6g.

g. Colocalization between CALB1 and ITGA1 from Fig. 6f. n=3, replicates defined as in Fig. 6d.

h. Representative confocal image of the DCN in P60 mice, demonstrating synaptic changes between Purkinje neuron synaptic termini and NEUN+ DCN neurons. Scale bar = 20 µm.

i,j. Quantification of images from Fig. 6h. For each large diameter DCN neuron we counted the number (i) and size (j) of CALB+ structures immediately adjacent to each DCN neuron using an automated analysis pipeline (see Methods). Replicates defined as in Fig. 6d, n=4, paired T-test.

k. Representative confocal image of DCN neurons, with NEUN channel overexposed to enhance projections. Closed arrowheads mark DCN neuron projections, open arrowhead DCN neuron soma. Scale bar = 20 µm.

l. Quantification of images from Fig. 6k. Projections were defined as small (5-15 µm diameter) NEUN+/DAPI- structures. Replicates defined as in Fig. 6d, n=4. Fig. S6f provides quantification of DCN neuron soma.

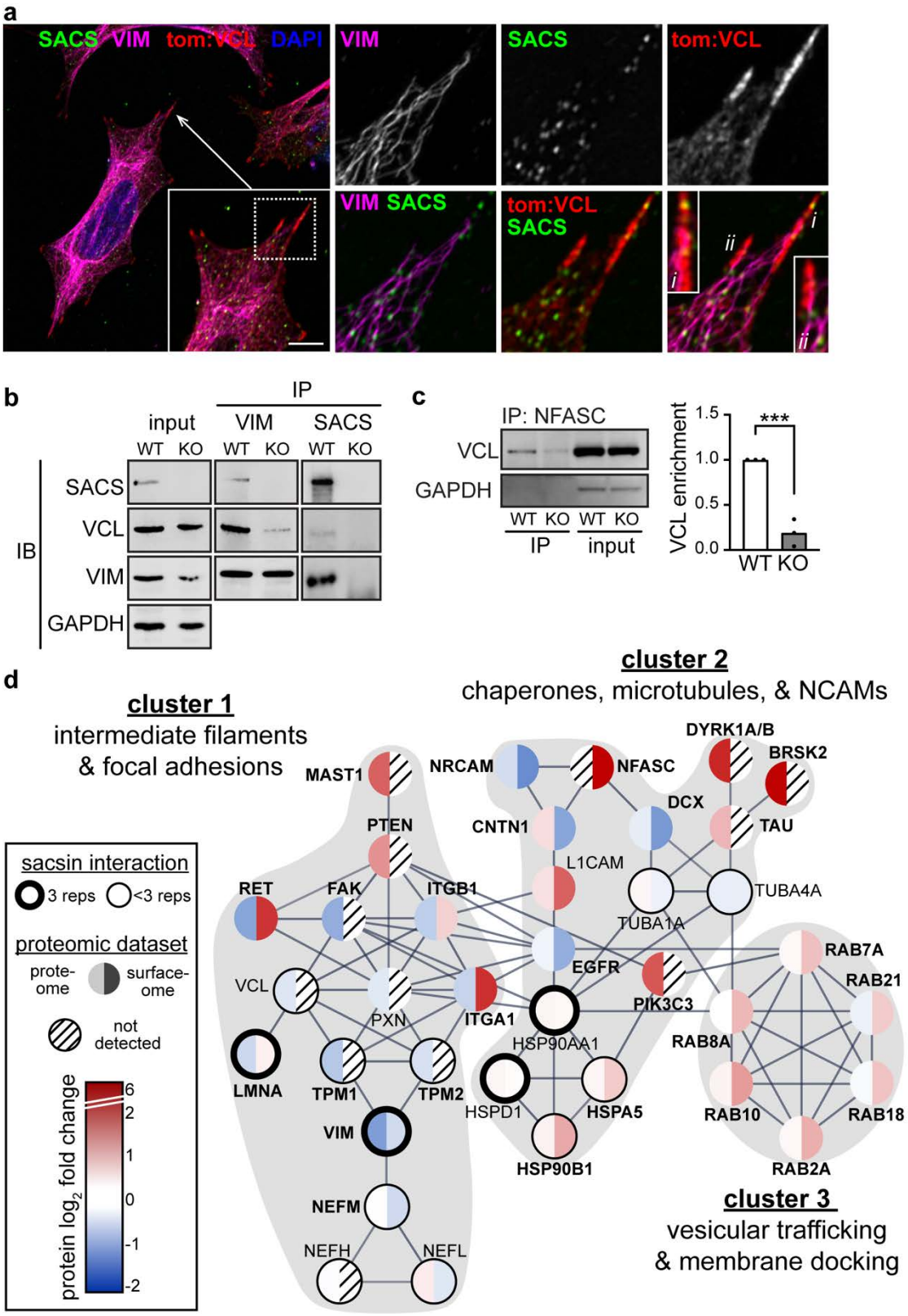

Figure 7 – The loss of sacsin disrupts protein-protein interactions

a. Representative Airyscan confocal analysis of sacsin, vimentin, and transfected tdTomato:vinculin staining in WT SH-SY5Y cells, demonstrating sacsin localization along vimentin tracts and focal adhesions. Scale bar = 10 µm.

b. Vimentin or sacsin were immunoprecipitated from WT and sacsin KO SH-SY5Y cells, and co-immunoprecipitated proteins (sacsin, vinculin, vimentin) were analyzed by western blot. Results suggest decreased interaction between vimentin and vinculin in sacsin KO cells.

c. Co-IP of NFASC and vinculin in WT and sacsin KO cells. Vinculin was not detected in secondary antibody only control blots (not shown), suggesting a specific interaction. Quantification of n=3 co-IP experiments shows the interaction between VCL and NFASC is greatly reduced in sacsin KO cells, despite NFASC being substantially overexpressed in *SACS* KO cells (Fig. 6d).

d. STRING protein interaction map depicting proteins identified across proteomics datasets. Lines between proteins indicate high confidence interactions (interaction score>0.7). We removed proteins with redundant interactions for clarity (for example most integrins have largely overlapping interactomes). Proteins identified in the sacsin interactome profiling are circled, with the thick circle marking interactors identified in all replicates, thin circle marking interactors identified in a subset of samples. Proteins are colored by $\log_2$ f.c. in proteome (left half) and cell surface proteome (right half). Striped lines indicate no detection. Clusters identified by k-means clustering are marked by grey background.

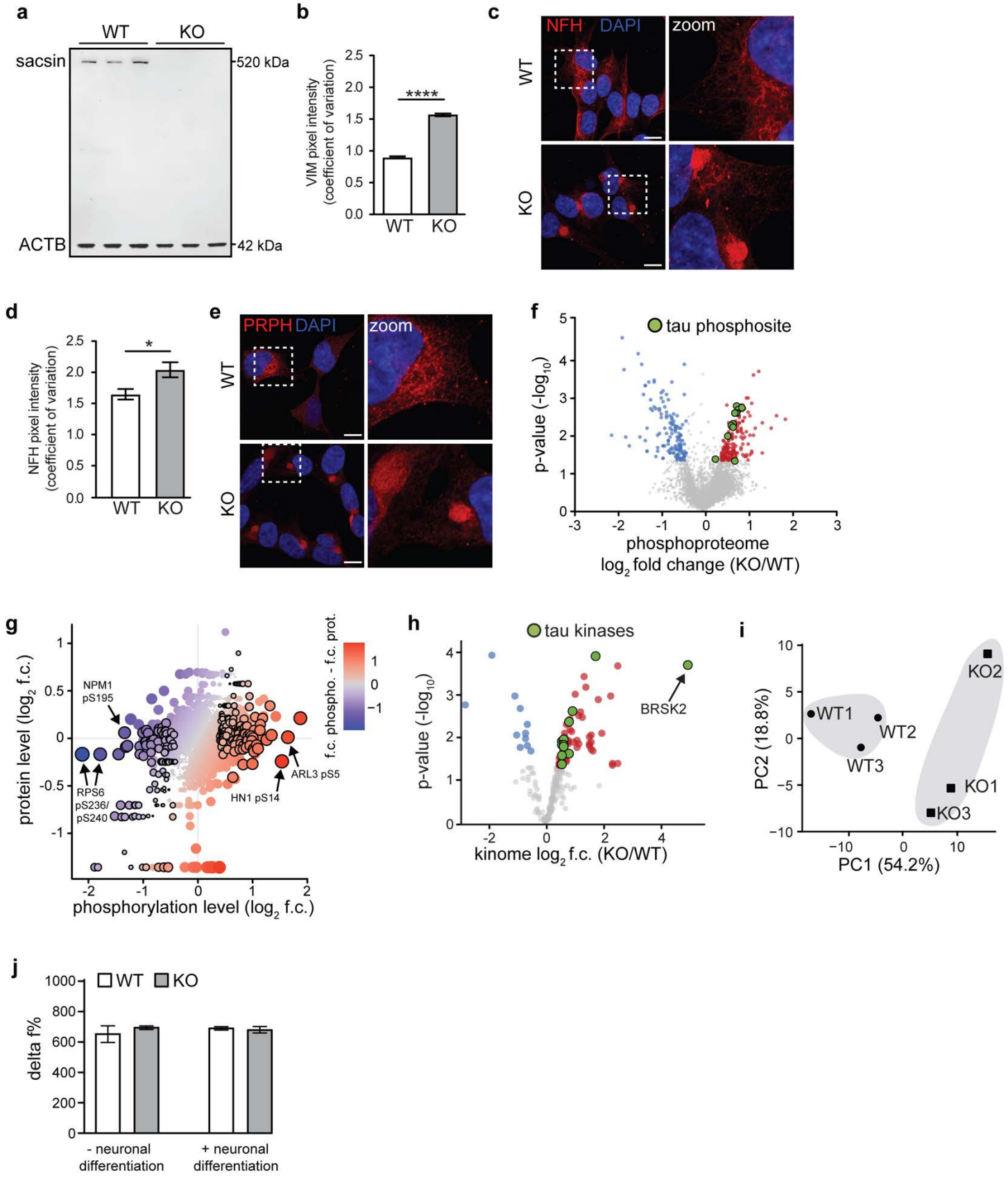

Extended Data Figure 1 – sacsin KO SH-SY5Y cells recapitulate cellular phenotypes consistent with known deficits

a. Western blot for sacsin and ACTB demonstrating the loss of sacsin in SH-SY5Y KO cells.

b. Coefficient of variation of vimentin pixel intensity values across the cell, with lower values indicating uniform distribution and higher values indicating polarized distribution.

c. Representative confocal images of WT and sacsin KO cells immunostained for the neurofilament heavy chain.

d. Coefficient of variation of NFH pixel intensity.

e. Representative confocal images of WT and sacsin KO cells immunostained for peripherin, an intermediate filament protein found in neurons in the peripheral nervous system.

f. Phosphoproteomic analysis of sacsin KO cells. Green circles mark specific phosphorylated residues on tau.

g. Phosphopeptide levels compared to changes in total protein levels. Color scale reflects the difference in $\log_2$ f.c. between each dataset. Black outline marks phosphosites with $p<0.05$ and $\log_2$ f.c. -/+0.4.

h. Kinome profiling of sacsin KO cells. Green circles mark kinases which are known to directly phosphorylate tau.

i. Principle component analysis of all kinases identified in kinome profiling data (Supp. Table 1). Unsupervised hierarchical clustering separated WT and KO cells (grey shading), suggesting widespread changes in the kinome of sacsin KO cells.

j. Biochemical analysis of tau aggregation using homogeneous time resolved fluorescence (HTRF) and anti-Tau antibodies conjugated with either Tb (donor) or d2 (acceptor) fluorophores. Graph represents the HTRF ratio, or Delta f%, of the two emission signals comparing WT/KO SH-SHY5Y lysates. n = 3.

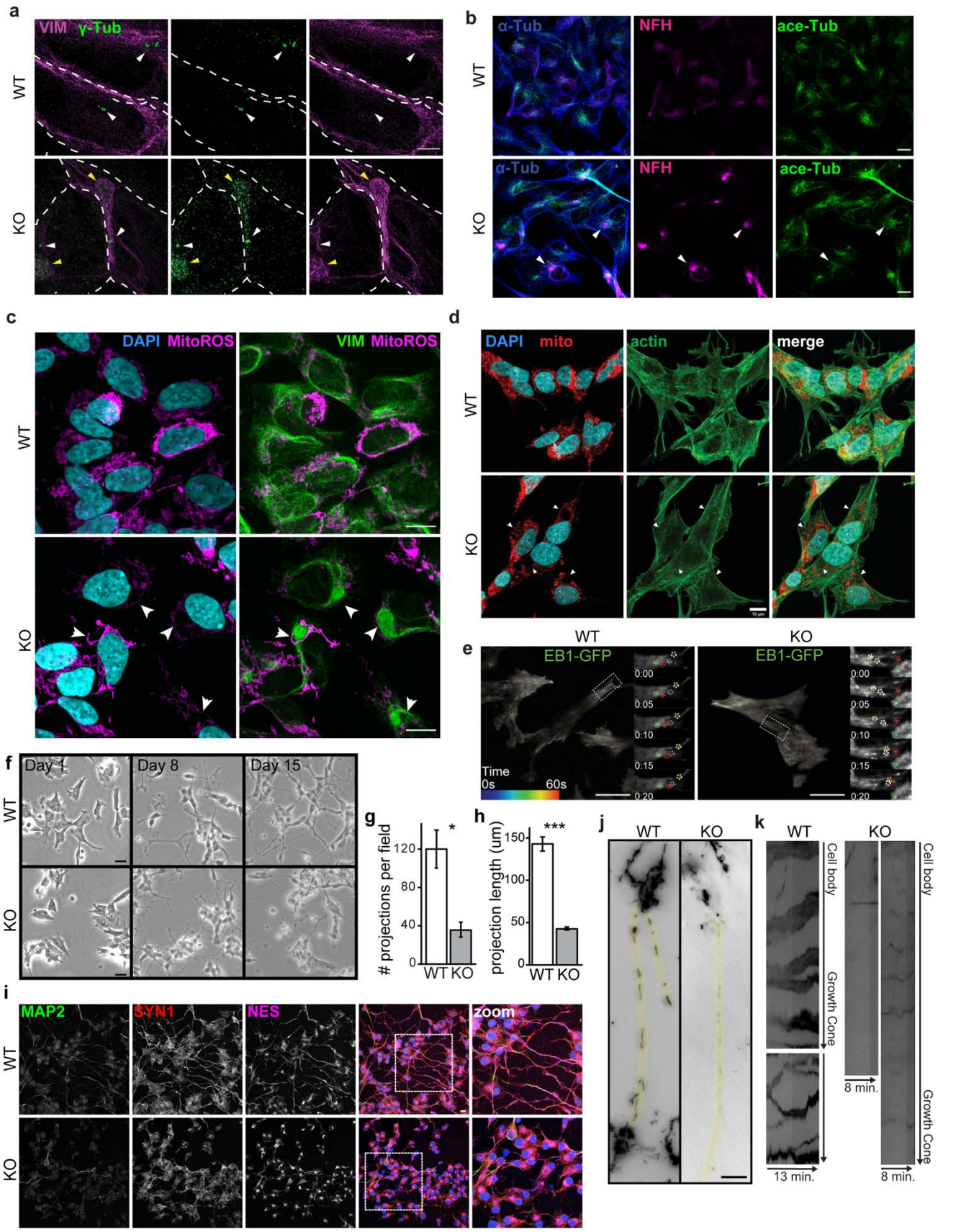

Extended Data Figure 2 – Microtubule and mitochondria deficits in sacsin KO cells

a. Super resolution structural illumination microscopy images showing accumulation of gamma-tubulin within perinuclear vimentin bundles of sacsin KO cells. White arrows point to centrioles, yellow arrowheads highlight the presence of gamma-tubulin within vimentin bundles in KO cells. Dashed white lines denote boundaries between adjacent cells. Scale bar = 1um.

b. Representative confocal images of immunostaining for alpha tubulin, neurofilament heavy, and acetylated tubulin in WT and sacsin KO cells. Arrowheads mark coincidence of acetylated tubulin and neurofilament bundles, suggesting that acetylated tubulin structures are found in proximity to neurofilament bundles, but also localize throughout the cell.

c. Representative confocal images of WT and sacsin KO cells stained for the mitochondria membrane potential dependent dye CMXRos, vimentin, and nuclei (DAPI). Arrowheads highlight the exclusion of mitochondria from vimentin bundles.

d. Representative confocal images of WT and sacsin KO cells immunostained for mitotracker, actin, and nuclei (DAPI). Arrowheads highlight the exclusion of mitochondria from vimentin bundles.

e. Representative TIRF microscopy images from WT and sacsin KO cells expressing EB1-GFP. Microtubule growth tracks are color coded marking their position over time. Insets show the enlargement of outlined regions and movement of individual comet movement over time (circles), numbers refer to seconds.

f. Representative phase contrast brightfield images of WT and sacsin KO cells across 15 days of neuronal differentiation.

g,h. Quantitation of the number of projections per field (g) and length of projection (h) of WT/KO cells demonstrating significantly reduced number and length of projections in sacsin KO cells.

i. Confocal images of WT/KO cells after 15 days in differentiation conditions, stained for neuronal markers microtubule associated protein 2 (MAP2) and synapsin1 (SYN1), and the intermediate filament protein nestin (NES), a marker of immature neurons. Scale bar = 10 μm.

j. Mitochondria labeled with mitoTracker GreenFM in neurites (highlighted in yellow) of 15 day differentiated WT/KO cells demonstrating the lack of elongated mitochondria in sacsin KO neurites. Images were snapshots from live-cell time-lapse imaging.

k. Kymograph illustrating mitochondrial transport along neurites of differentiated WT/KO cells. Note that mitochondrial undergo both retrograde and anterograde movement in control but are relatively static in sacsin KO cells. Scale bar = 10 μm.

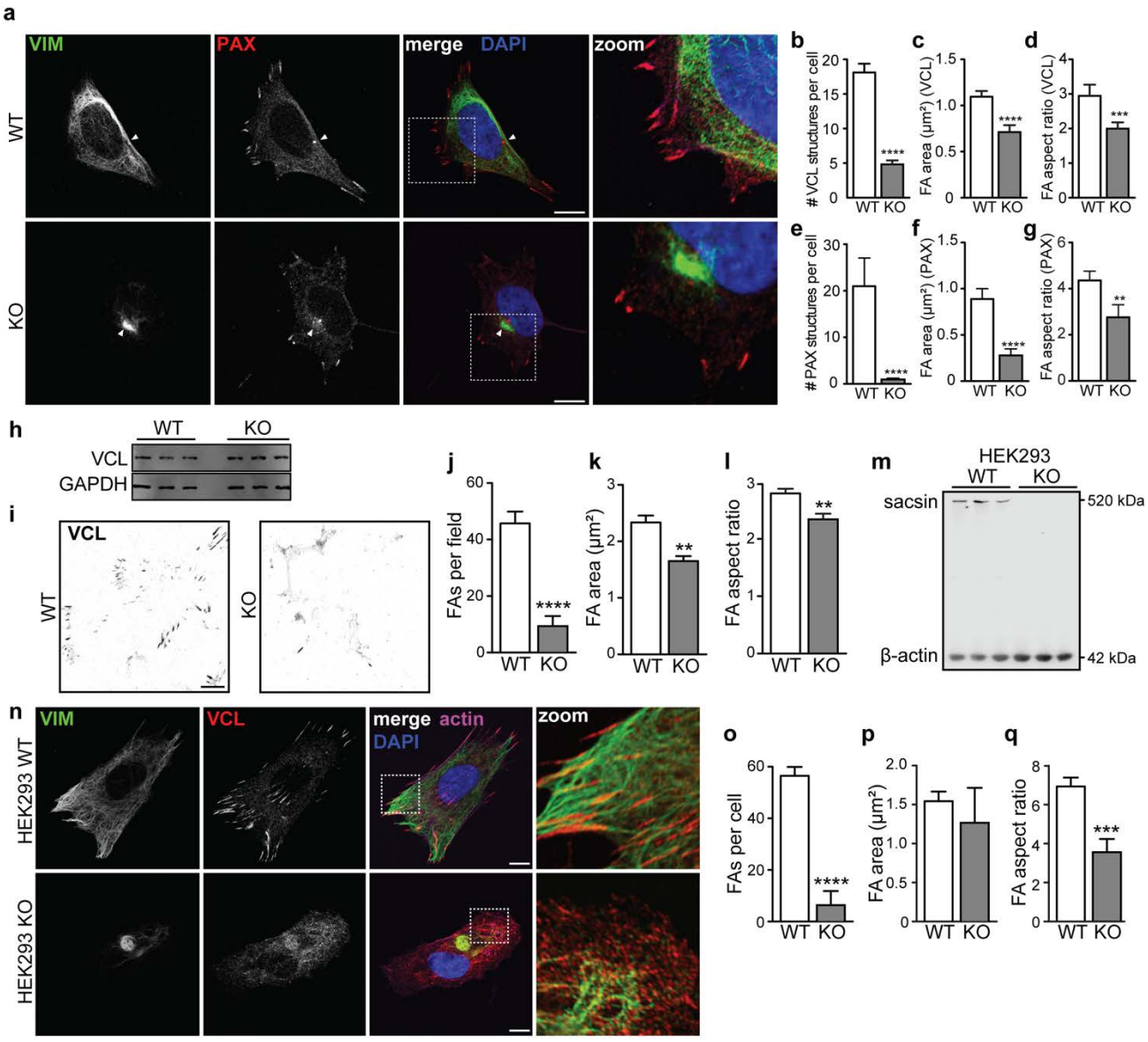

Extended Data Figure 3 – Focal adhesions are disrupted in sacsin KO cells

a. Representative confocal image of WT/KO cells labelled with vimentin and paxillin. Arrowhead marks the PAX positive MTOC, which is sequestered in the vimentin bundle in *SACS* KO cells. Scale bar = 10 µm.

b-g. Quantification of images from Fig. 3c (b-d), and Extended Data Figure 3a (e-g). Aspect ratio = width:height ratio. n=3 independent replicates.

h. Western blot for vinculin, showing that levels of the focal adhesion protein are unaltered in KO cells.

i. Representative image of cover slips treated with hypotonic shock to remove cell bodies, leaving focal adhesions retained through ECM interaction. Staining for the focal adhesion protein vinculin. Scale bar = 10 µm.

j-l. Quantification of the incidence, area, and aspect ratio of paxillin positive focal adhesions in WT/KO cells.

m. Western blot for sacsin and ACTB demonstrating the loss of sacsin in HEK293 KO cells.

n. Confocal images of HEK293 cells immunolabeled for vimentin, vinculin, and actin. Scale bar = 10 µm.

o-q. Quantification of images from Supp. Fig. 3n, suggesting focal adhesion deficits are consistent with SH-SY5Y cells.

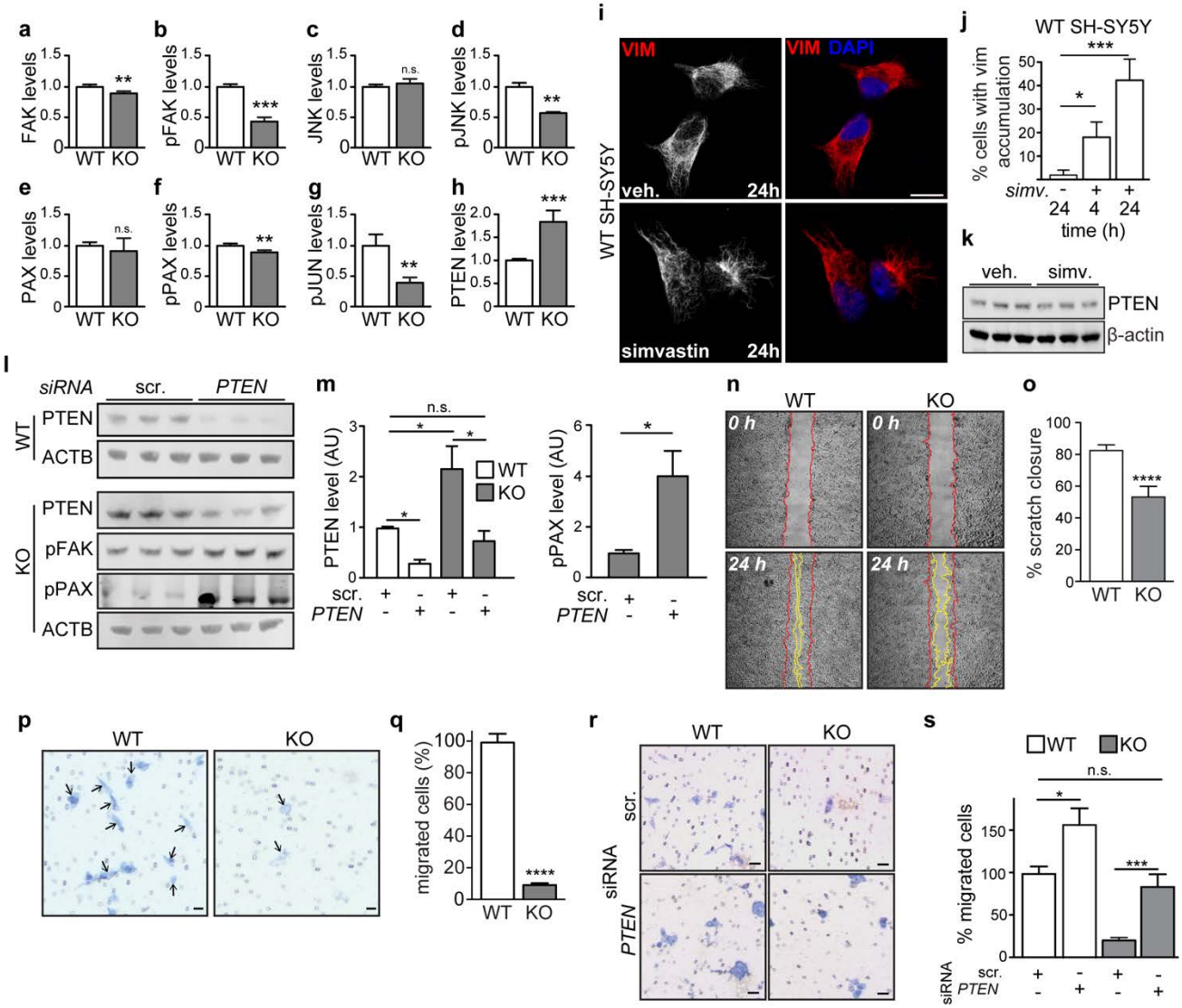

Extended Data Figure 4 – Modulating *PTEN* rescues cellular phenotypes in sacsin KO cells

a-h. Quantification of immunoblots from Fig. 4c. Intensity normalized to ACTB. n=3 biological replicates.

i. Representative confocal images of the induction of vimentin bundling by simvastin. Scale bars = 10 μm.

j. Quantification of vimentin bundling phenotype induced by simvastin over time.

k. Western blot of PTEN levels in 24-hour simvastin treated WT cells, suggesting that vimentin bundling does not affect PTEN levels.

l. Western blots of WT/KO cells treated with siRNAs targeting *PTEN* or scrambled.

m. Quantification of PTEN and pPAX levels in WT/KO cells treated with scrambled or *PTEN* targeting siRNAs, suggesting *PTEN* is returned to WT levels in sacsin KO cells. n=3.

n,o. Representative bright field images of a scratch assay of WT/KO SH-SY5Y cells. Red and yellow lines mark the edge of the wound after 0 and 24 hours of recovery, respectively (n). Quantification of scratch closure in WT/KO 24 hours after the scratch was made, n=3 (o).

p,q. Representative images of WT/KO SH-SY5Y cells in Transwell chambers with 8 μm pores 24 hours after plating, fixed and stained with Giemsa blue. Arrows mark cell bodies, scale bar = 20 μm (p). Quantification of the number of migrated cells after 24 hours, normalized to WT, n=3 (q).

r-s. Representative images of WT/KO SH-SY5Y cells transfected with the indicated siRNAs, and plated in Transwell chambers. Scale bar = 20 μm. (r). Quantification of Transwell assay 24 hours after plating. n=5 per cell line (s).

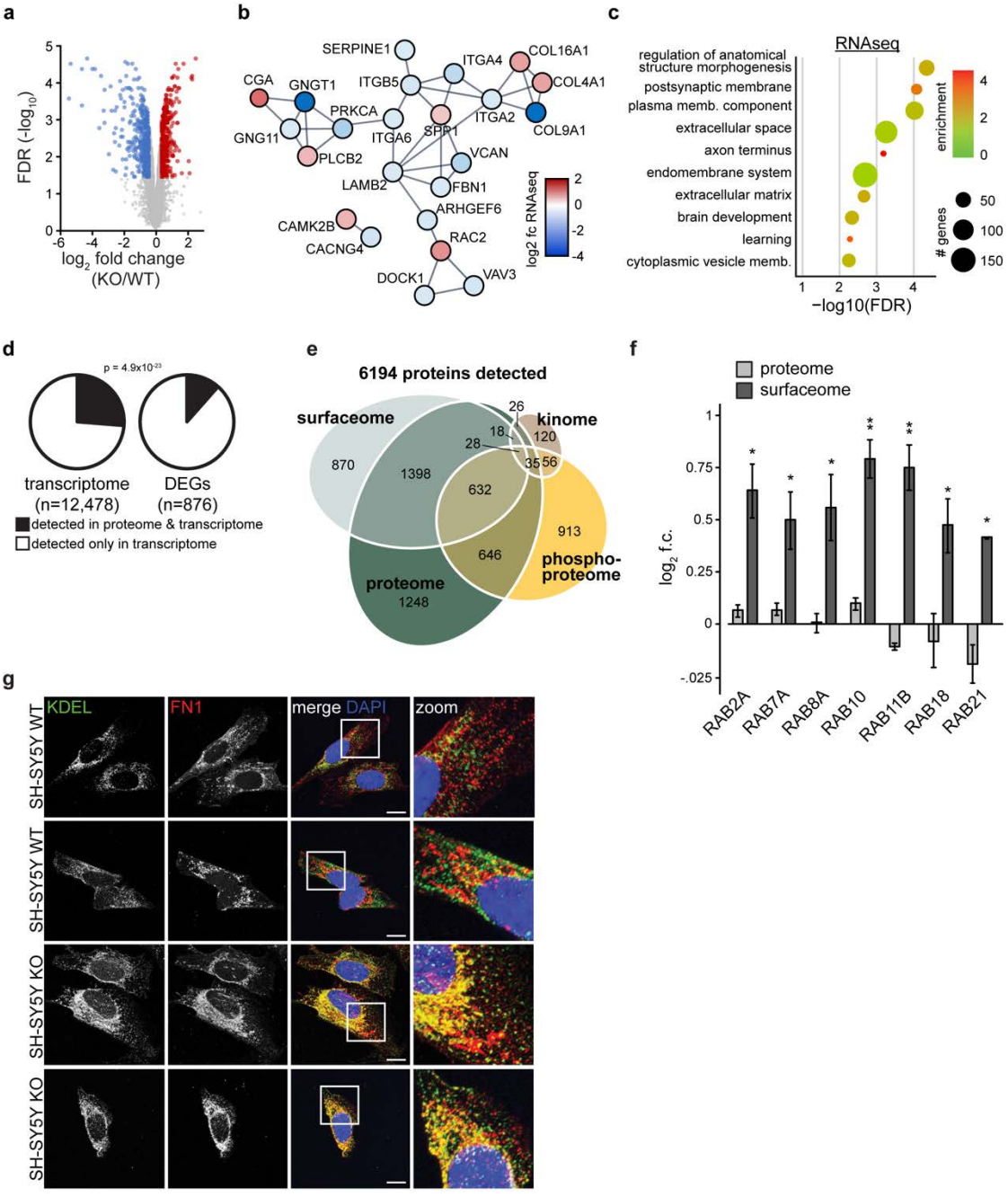

Extended Data Figure 5 – Altered transcription of synaptic adhesion and vesicular proteins

a. RNA-seq of 15 day neuronally differentiated SH-SY5Y cells.

b. Interaction network of cell adhesion proteins that are differentially expressed.

c. GO term analysis of differentially expressed genes suggests that synaptic and vesicular transport genes are altered in neurons ($p<0.05$, $\log_2$ f.c. -/+ 0.5).

d. Overlapping gene/protein identification from RNAseq and proteomics, showing that DEGs were not detected as readily in proteomics, as proteins that were not differentially expressed at the RNA level. Hypergeometric test was used to calculate enrichment p-value.

e. Euler diagram of protein identification across all mass-spec datasets.

f. $\log_2$ f.c. of Rab proteins in proteome and surfaceome datasets. Asterisks refer to statistical significance in each dataset. No Rabs were significantly affected in the proteome.

g. Representative confocal images of cells immunolabelled for fibronectin and KDEL in in WT/KO SH-SY5Y cells. Scale bar =10 μm.

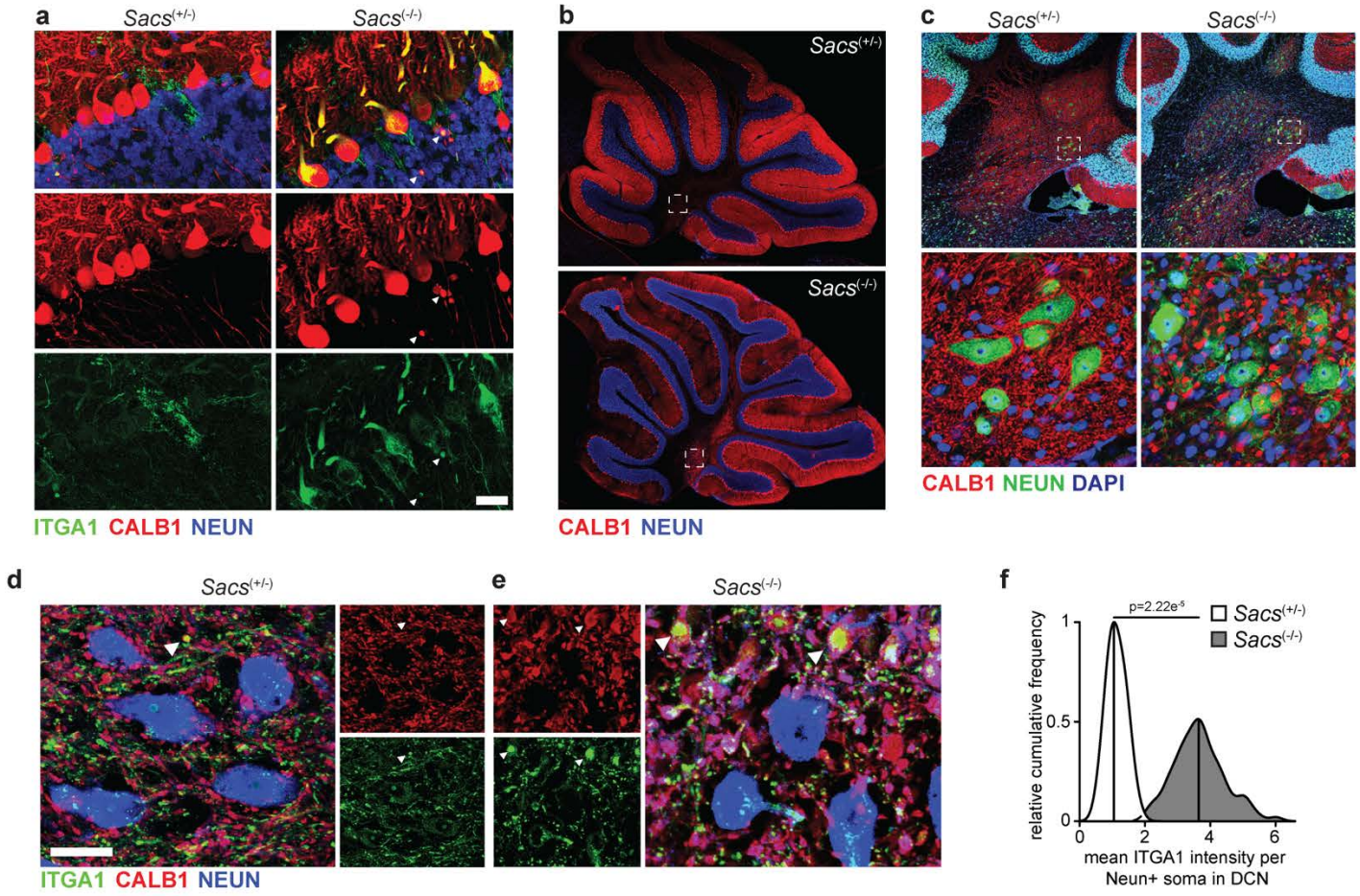

Extended Data Figure 6 – Cerebellar imaging in *SACS* KO mice

a. Purkinje cell layer in P120 mice. Arrowhead marks ITGA1 accumulation in axonal swellings. Scale bar = 20 μm.

b. Sagittal cerebellar section, marking the general DCN region analyzed in Figs. 6h-l, S6c-f.

c. DCN in P120 mice, demonstrating substantial disruption of Purkinje neuron termini on DCN neurons. Scale bar = 20 μm.

d,e. DCN in P60 mice. Arrowheads mark large CALB1+ structures, with accumulation of ITGA1. Scale bar = 20 μm.

f. Quantification of images in Fig. 6k. Large diameter DCN neuron soma defined as NEUN+/DAPI+ where diameter is between 20-25 μm. Replicates defined as in Fig. 6d, n=4.

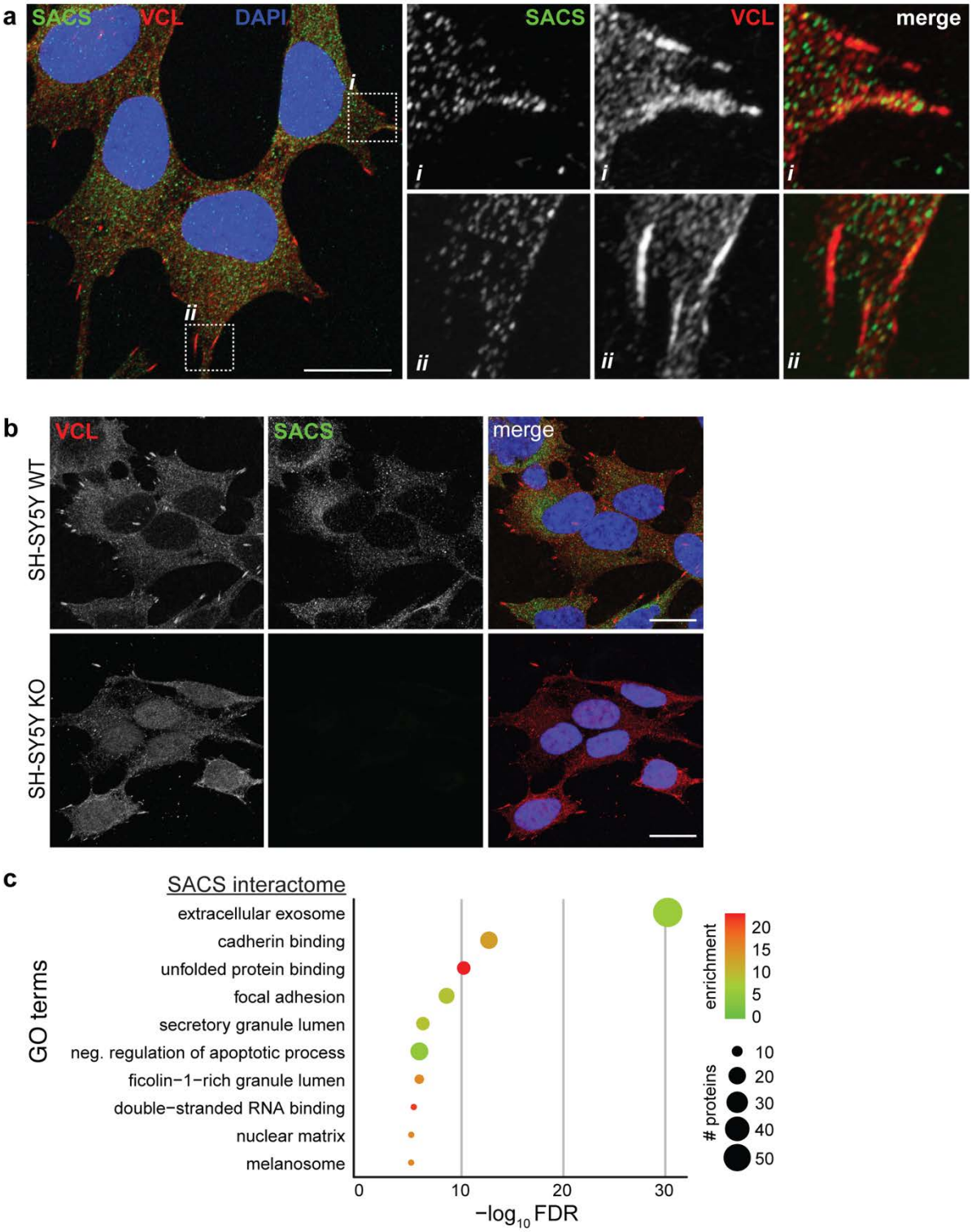

Extended Data Figure 7 – sacsin interactors

a. Representative confocal image for sacsin and vinculin in WT SH-SY5Y cells demonstrating sacsin colocalizes with focal adhesions.
b. Representative confocal image for sacsin KO cells processed in parallel to (a), demonstrating the specificity of sacsin staining.
c. GO term analysis of all proteins identified in the sacsin co-IP interactome (Supplementary Table 4).